2023

Nutrient Input in the Chagos Archipelago - the Controlling Mechanisms of Chlorophyll-a Distribution

Cairns, Harvey

UNIVERSITY OF PLYMOUTH

Nutrient Input in the Chagos Archipelago - the Controlling Mechanisms of Chlorophyll-a Distribution

by

Harvey Cairns

A thesis submitted to the University of Plymouth in partial fulfilment for the degree of

Research Masters

School of Biological and Marine Sciences

September 2022

Author's Declaration

At no time during the registration for the degree of Research Masters has the author been registered for any other University award without prior agreement of the Doctoral College Quality Sub-Committee.

Work submitted for this research degree at the University of Plymouth has not formed part of any other degree either at the University of Plymouth or at another establishment.

A programme of advanced study was undertaken, which included the taught modules MAR513 ‘Research Skills and Methods’ and MAR518 ‘Remote Sensing and GIS’.

Word count of main body of thesis: 8133

Signed: H Cairns

Date: 30/09/2022

Revised Word Count: 8873

Date:15/03/2023

Abstract: Nutrient Input in the Chagos Archipelago - the Controlling Mechanisms of Chlorophyll-a Distribution – Harvey Cairns

Phytoplankton primary productivity is vital in supporting the marine trophic system, and an understanding of the nutrient sources facilitating this is critical for informing conservation management.

Using a combination of *in situ* and remotely sensed data, we assess the contributions of different nutrient sources and corresponding productivity in a tropical island ecosystem free from anthropogenic nutrient pollution at varying temporal scales. Beyond the near-shore, annual mean normalised fluorescence line height (nFLH, a proxy for chlorophyll-a concentration) was 27% higher in shallow water (approx. 20m) than deep water (>5000m), demonstrating a chlorophyll-a enhancement in shallow waters. Linear regression revealed a significant (p=<0.001, N=852) relationship where increasing sea surface temperature (SST) was associated with decreasing nFLH. The same relationship was also found between SST anomaly and nFLH anomaly. These relationships were stronger in shallow water (R^2=0.39 for SST and nFLH, and 0.18 for the anomaly) than deep water (R^2=0.17 for SST and nFLH, and 0.10 for the anomaly), indicating shallower waters are more sensitive to strengthened stratification. Elevated SST is often associated with strengthened stratification, restricting entrainment from below the thermocline, and therefore restricting the movement of nutrients to the surface waters.

In situ CTD measurements revealed a highly stratified environment, with a steep pycnocline. In the mouth of Egmont Atoll, the flood tide was, on average, cooler (by 0.07°C) and more saline (by 0.025 PSU) than the ebb tide (two-sampled t-test, p=<0.001). This represents a change in water properties towards those below the pycnocline, suggesting tidally driven mixing is entraining water from below the surface mixed layer. However, no significant difference was observed in nitrate concentration. Instead, nitrate concentration was associated with salinity. Decreases in salinity were associated with increases in nitrate, following precipitation with an approximately 2-day lag, indicating that precipitation-driven surface runoff is a key nutrient source in waters adjacent to land.

Overall, results suggest that high-frequency, short-term variability in nitrate concentration is driven by precipitation, with longer term productivity variability governed by the strength of stratification, and consequential restriction of entrainment.

Table of Contents

List of Figures:

List of Tables:

Introduction:

1.1. Marine Productivity in the Chagos Archipelago:

The Chagos Archipelago or British Indian Ocean Territory (BIOT) is situated in the centre of the Indian Ocean at the southern end of the Chagos-Laccadive Ridge (Figure 1). It is a group of 5 atolls, comprised of over 60 islands and forms one of the largest marine protected areas in the world (Hays *et al.*, 2020), with a total area of 640,000km^2 (approximately 3 times the surface area of Great Britain); of which 6,000km^2 is shallow reef (Sheppard *et al.*, 2012), and the remainder being oceanic waters reaching maximum depths >5000m. Because of this, a wide variety of habitat types and seabed features are present within the MPA, making it important for both reef-dwelling and pelagic fauna (Koldewey *et al.*, 2010).

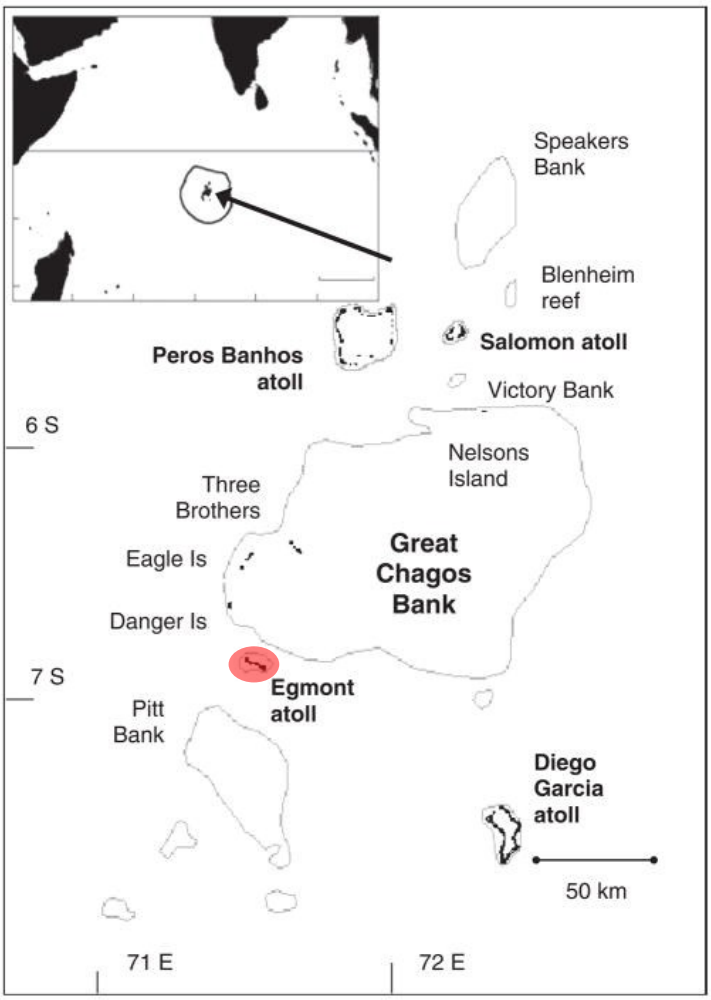

Figure 1: The Chagos Archipelago, inset map shows the location within the Indian Ocean and the MPA boundary. The study region is highlighted in red. Reprinted from Sheppard et al. (2012).

The archipelago has been uninhabited since the 1970's, with the exception of Diego Garcia atoll, which contains a US military base. It is the least polluted inhabited atoll in the world (Sheppard *et al.*, 2012), as well as the world's largest and most isolated atoll complex

(Sheehan *et al.*, 2019). The lack of anthropogenic pollution (Painting *et al.*, 2019, 2021) means that the Chagos Archipelago provides a unique opportunity to observe the impact of oceanographic processes on the marine ecosystem across a variety of spatial and temporal scales, almost entirely free of localised anthropogenic interference.

Marine primary production is essential for sustaining ocean life across all trophic levels. The Chagos Archipelago experiences elevated levels of primary production (Hosegood *et al.*, 2019), compared to the surrounding ocean which is oligotrophic (Morel, Claustre and Gentili, 2010). In oligotrophic regions, primary production is limited by nutrient availability. There are two key nutrient sources in the Chagos Archipelago currently documented, the first being year-round upwelling at the Seychelles-Chagos Thermocline Ridge (SCTR, see figure 4) (Hermes and Reason, 2009; Zhang and Han, 2019), the second being terrestrial runoff, enhanced by seabird guano. Graham et al. (2018) and Benkwitt et al. (2019) both recognise seabird guano, carried into the ocean by terrestrial runoff, as a key nutrient source, specifically in localised waters immediately surrounding bird-inhabited islands. There is currently no clear evidence for which nutrient source is dominant, prohibiting an assessment of how the ecosystem may respond to changes in the oceanographic environment with climate change, such as the globally deepening and intensifying thermocline (Sallée *et al.*, 2021).

Several other physical oceanographic processes can drive primary production, each with their own controlling climate mechanisms (such as elevated winds/precipitation) that can enhance/suppress their impact. The island mass effect is a near-ubiquitous process at island coral reef ecosystems (Gove *et al.*, 2016), although as yet there is no evidence of this in the Chagos Archipelago. Upwelling is known to occur in the region in the form of the SCTR, however there is a lack of evidence for localised upwelling/entrainment of nutrients that would explain the elevated primary production. The climate processes that impact the Chagos Archipelago are known (see section 1.3), but their respective impacts on primary production on a more local scale than the SCTR are also unknown.

1.2. Mechanisms Governing Nutrient Availability:

Surface nitrate concentrations, especially in the oligotrophic ocean, are generally extremely low. However, this concentration typically increases below the thermocline (Garside, 1985; Lewis *et al.*, 1986), with the concentration at depth significantly higher. This results in

stratification playing a key role in limiting surface productivity, by restricting the vertical transport of nitrate to the surface.

1.2.1. Island Mass Effect:

The Island Mass Effect (IME) is a broad term that encapsulates the process of enhanced primary production surrounding an island ecosystem, driven by both land-derived and ocean-derived nutrients (Figure 2). This enhancement of production is usually seen in the wake of the island (Figure 3), as the current carries nutrients and phytoplankton downstream (Hernández-León, 1991; Gove *et al.*, 2016). This can be driven by several processes (often a combination of multiple), such as: current-bathymetry interaction, downstream mixing, and eddies in the wake of land masses, internal waves, lagoon/atoll flushing, and surface runoff (Doty and Oguri, 1956; Hamner and Hauri, 1981; Gove *et al.*, 2016). These processes can cause up to an 86% increase in phytoplankton biomass over oceanic conditions (Gove *et al.*, 2016). The influence of the IME has been found to propagate beyond the surface, influencing phytoplankton concentration across the full euphotic zone (Gove *et al.*, 2016; James *et al.*, 2020). Whilst the IME is a persistent feature in the locations where it occurs, elements of it can be enhanced/suppressed by external factors such as wind speed and rainfall, which are drivers of surface runoff and wind-induced turbulent mixing and wind-driven currents (Martinez and Maamaatuaiahutapu, 2004; Messié *et al.*, 2020).

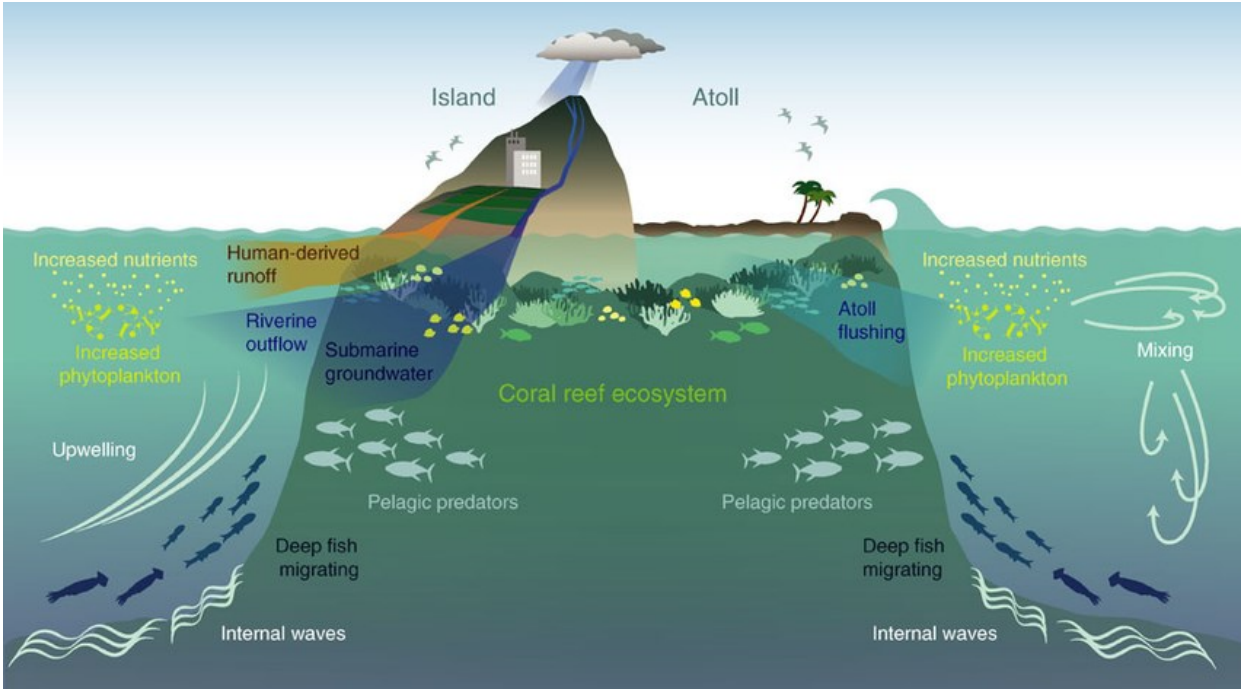

Figure 2: The causes and impacts of the Island Mass Effect. Reprinted from Gove et al. (2016)

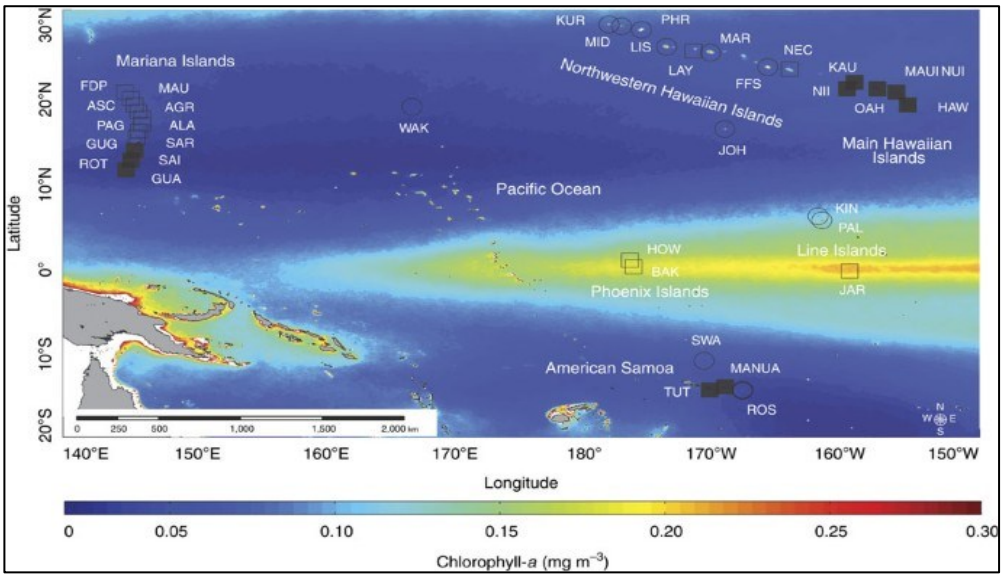

Figure 3:10-year mean chl-a concentration, with the IME shown in the wake of islands in the Pacific Ocean. Reprinted from Gove et al. (2016)

For the purpose of this study, processes of the IME will be considered separately as land-derived nutrient input (surface runoff) and ocean-derived nutrient entrainment (upwelling, bathymetry driven mixing, internal waves etc.).

1.2.2. Upwelling and Deep-Water Nutrient Entrainment:

The large-scale upwelling across the SCTR is a well-studied phenomenon, regarded as important in controlling regional climate, the Indian Ocean Dipole (IOD, a regional climate oscillation), and nutrients in the upper ocean (Hermes and Reason, 2008, 2009). The SCTR (Figure 4) is a dome-like feature in the thermocline, in the region of 55°E-65°E, 5°S-12°S with a depth range of ~80-100m (Hermes and Reason, 2008), maintained by large-scale wind stress curl, and also influenced locally by divergence between south-easterly trade winds and monsoon westerly winds (Hermes and Reason, 2008).

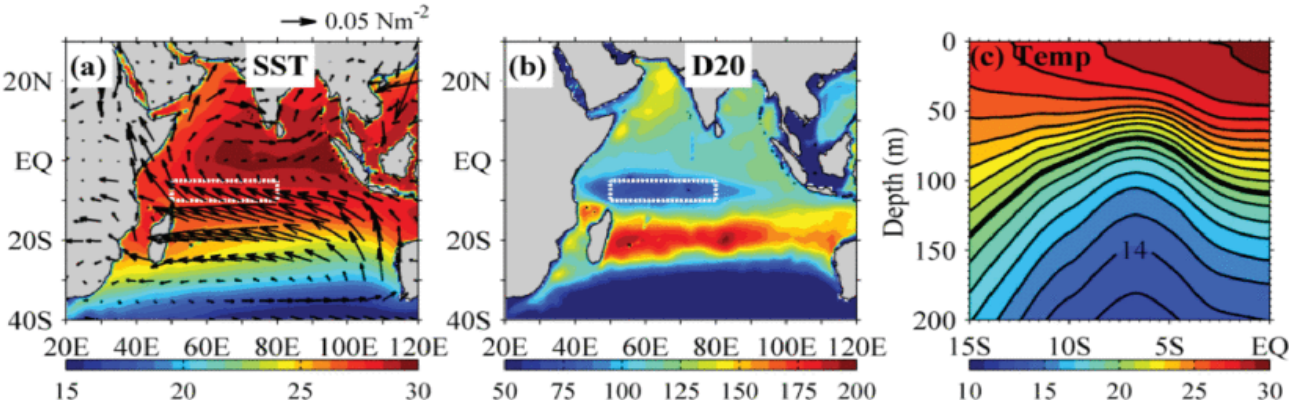

Figure 4: Annual mean (a) SST (colour shading, °C) and wind stress (vectors, N·m2) (b) Thermocline depth (m) (c) Latitudinal variation of annual mean temperature (°C) in the upper 200 m averaged over 50°E–80°E. Contour interval is 1 °C. The thermocline depth (20 °C isotherm) is highlighted. White boxes show the SCTR (5°S–10°S, 50°E–80°E). Reprinted from Nyadjro et al. (2017).

Zhang and Han (2019) attribute the IOD as a key factor in controlling upwelling strength at the SCTR. In the neutral IOD phase, westerly winds blow across the Indian ocean, and upwelling at the SCTR is 'normal'. A positive IOD induces warming of the Tropical Southwestern Indian Ocean (Praveen Kumar *et al.*, 2014), increasing convection at the SCTR, slowing the westerly winds, allowing for upwelling in the Eastern Indian Ocean, and driving downwelling at the SCTR, suppressing the usual upwelling in the region. This is then reversed in the negative phase, enhancing the upwelling at the SCTR.

Mixed layer depth (MLD) is also a controlling factor of nutrient entrainment, with the strength of nutrient entrainment being driven largely by mixed layer depth (MLD) and degree of stratification; when a deep MLD reaches the nutricline, nutrient rich water is entrained to the surface, driving primary production (Carranza and Gille, 2015; George *et al.*, 2018; Rigby *et al.*, 2020). Elevated wind speeds contribute to a deepening of the MLD, and the opposite is true of weaker winds; with the suppression of turbulent mixing allowing for a shoaling of the mixed layer (Kataoka *et al.*, 2019). Despite the presence of a year-round shallow thermocline at the SCTR, George et al. (2018) found an elevation in surface chlorophyll-a was only experienced between June and October, due to the deep mixed layer experienced during this period, contributed to by wind-driven mixing deepening the mixed layer.

Increasing SST often increases thermal stratification of the ocean, and often occurs alongside a shoaling of the mixed layer depth (Dunstan *et al.*, 2018). This shoaling of the MLD causes the SML to be more sensitive to incoming shortwave radiation, raising SST further (Kataoka *et al.*, 2019) by effectively reducing the volume of water into which the incoming radiation is absorbed. In this highly stratified environment, vertical entrainment of nutrient-rich deep water becomes limited, and primary productivity is also limited as a result (Dave and Lozier, 2010; Hsu, Feng and Wijffels, 2021). It would therefore be expected that an increasing SST would correspond with an increasingly stratified surface layer, which would be associated with nutrient limitation due to restricted entrainment, inhibiting primary production.

The presence of localised upwelling in Chagos on a smaller scale than the SCTR is undocumented, potentially due to a lack of modelling at a suitable resolution. However, bathymetry driven upwelling is a common feature amongst many other isolated archipelagos (Anderson, Adam and Goes, 2011). In the Maldives, phytoplankton blooms were found to be driven by monsoon-driven currents passing over the Maldives Ridge, lifting nutrient-rich

deep water to the photic zone (Anderson, Adam and Goes, 2011). This is of relevance to the Chagos Archipelago, as the Maldives Ridge is a section of the Laccadive Ridge, upon which the Chagos Archipelago is also situated. The Chagos Archipelago is subject to many of the same climate processes that are driving the currents in the Maldives, such as the switching monsoons, suggesting that similar processes could be facilitated in the Chagos Archipelago too.

1.2.3. Internal Wave Mixing and Related Mechanisms:

Internal waves can influence nutrient concentrations in surface waters by causing the mixing of sub-thermocline waters into the surface mixed layer (Reid *et al.*, 2019; Whalen *et al.*, 2020). It is understood that internal waves play a role in governing primary production at the SCTR (Hermes and Reason, 2009) as well as driving biomass distributions within the Chagos Archipelago (Hosegood *et al.*, 2019). On a large scale, equatorial Rossby waves propagating across the Indian ocean have been found to impact the depth of the SCTR (Webber *et al.*, 2014; Zhang and Han, 2019), with upwelling (downwelling) Rossby waves causing the SCTR to be anomalously shallow (deep) (Hermes and Reason, 2009). On a smaller scale, internal lee waves have been found to flush seamount crests with cool water (Hosegood *et al.*, 2019), and although nutrient concentrations were not reported, it is likely that this cooler deep water would have also been nutrient-rich and could be a driver of nutrient transport into the photic zone if a mechanism able to transport nutrients upwards was present.

1.2.4. Land-Derived Nutrient Input:

Seabird guano is recognised as a key nutrient source in coastal waters (Graham *et al.*, 2018; de La Peña-Lastra, 2021). The Chagos Archipelago is an important bird habitat, with 175,000 breeding pairs of seabirds visiting the archipelago each year (Chagos Conservation Trust, no date). These seabirds were found to be a crucial provider of nitrogen and phosphorus to reefs, aiding in their recovery after bleaching events by increasing the rate of herbivory and preventing macroalgal dominance over coral (Benkwitt, Wilson and Graham, 2019).

Graham et al. (2018) found seabird density in the Chagos Archipelago to be 760 times higher on islands where humans had not introduced the invasive black rat (*Rattus rattus*), and terrestrial nitrogen deposition rate to be 251 times higher as a result, which is important as nitrogen is a limiting element for biological productivity in oligotrophic oceans (Ryabenko,

2013). The leaching of these nutrients into the waters of the archipelago via terrestrial runoff led to a higher value of nitrogen stable isotope δ15N being found in macroalgae, turf algae and filter-feeding sponges. Fish communities on reefs adjacent to rat-free islands were also found to have a 48% higher overall biomass. These findings are consistent with a similar study that took place on islands off the New Zealand coast, where Fukami et al. (2006) found that rat-infested islands had lower soil fertility, and the adjacent reefs had lower nutrient levels as a result.

Given this knowledge of land-based nutrient leaching impacting adjacent reefs, it can be inferred that processes which drive the transport of terrestrial nutrients into the ocean would trigger an elevation in nutrients. Rainfall induced surface runoff is known to drive primary production by washing terrestrial nutrients into coastal waters (Zheng and Tang, 2007; Shatova *et al.*, 2016).

1.3. Climate Scale Atmospheric Drivers of Nutrient Availability in the Chagos Archipelago:

Both surface runoff and wind-driven upwelling are driven by atmospheric conditions, and there are many atmospheric systems which all govern rainfall and surface winds in the Chagos Archipelago. The Madden-Julian Oscillation (MJO) is a climate oscillation repeating on a 30–60-day cycle across the Indian Ocean (Zhang, 2005). It forms as a region of enhanced cloud cover, winds, and rainfall over the east coast of Africa, propagating eastward across the Indian Ocean, Indonesia, and the Western Pacific, ending over the Central Pacific Ocean. As the MJO brings elevated wind and rainfall, it provides conditions that are conducive to enhancing the IME in the Chagos Archipelago as it passes over, driving surface runoff and wind-induced mixing.

The Indian Ocean Dipole (IOD) is a basin-scale irregular oscillation that impacts weather from the East Africa, across the Indian Ocean to West Australia (Saji *et al.*, 1999). It is measured as the Dipole Mode Index (DMI) which is the east-to-west sea surface temperature gradient across the tropical Indian Ocean. The DMI is divided into 3 phases: positive, neutral, and negative. When in the positive phase, the Western Indian Ocean is warmer than the Eastern Indian Ocean, and experiences increased convection and rainfall as a result, whilst the opposite is true in the negative phase (Saji *et al.*, 1999).

El Niño-Southern Oscillation (ENSO) has been found to be closely related to Southwest Indian Ocean thermocline variability. Whilst the direct impacts of ENSO are mainly focussed in the Pacific Ocean, it has far-reaching processes that impact the Chagos Archipelago and the SCTR. For example, when an El Niño event occurs, anomalous westerly winds are caused across the equatorial Indian Ocean. These winds then cause a downwelling Rossby wave, which propagates westward across the Indian Ocean (Xie *et al.*, 2002), causing downwelling at the SCTR.

1.4. Assessing Chagos Archipelago Productivity using Remote Sensing and Numerical Model Output:

Due to the remote nature of the Chagos Archipelago, many studies of the region (e.g., Graham et al., 2018; Head et al., 2019) take nutrient and chlorophyll data from remote sensing platforms or global ocean models. In the instance of a stratified oligotrophic region like the Chagos Archipelago, remote sensing is unable to detect chlorophyll throughout the extent of euphotic zone; it is typically limited to the upper 10-20m of the water column (Gordon and McCluney, 1975). The Chagos Archipelago and the Western Tropical Indian Ocean region is known to have a deep chlorophyll maximum (DCM) at around 50-75 metres (George *et al.*, 2012, 2018; Fasolo, 2013), beyond the range of detection by ocean colour satellites (Cornec *et al.*, 2021). This means that this data can be used as a reflection of surface chlorophyll only, and does not accurately show the spatial distribution of chlorophyll within the surface mixed layer as a whole (Raitsos *et al.*, 2013).

Global ocean models are also of limited use. The coarseness of these models (0.5° resolution in the case of Graham et al., 2018) makes them unsuitable for resolving localised processes that may be critical to nutrient supply occurring in the order of hundreds of meters from the coast.

A drawback to the Graham et al. (2018) study was the model used to estimate many key values. Biomass, production, and size structure of consumers in the waters surrounding the islands were calculated from the primary production available to support them, and water temperature. These factors were estimated from annual mean values during 2010-2012; during this time the IOD was mostly in the positive phase, which would mean that sea surface temperatures were elevated, and that primary production was reduced (Goes, 2020) as a result of atmospheric forcing reducing upwelling. Additionally, chlorophyll concentration

and primary production were obtained from a model with a 0.5° spatial resolution, a coarse resolution when examining processes happening on a much finer scale.

1.5. Aims and Objectives:

The presence of basin scale upwelling in the Chagos Archipelago region is well documented in the form of the SCTR. This upwelling is governed by the IOD, and Rossby waves associated with ENSO, which can enhance or suppress the SCTR. Mixing within the surface layer is important for the entrainment of nutrients from the SCTR to the surface. It remains unknown whether upwelling on a smaller scale (i.e., bathymetry driven upwelling) occurs within the archipelago, although this feature is present at other locations along the Chagos-Laccadive ridge.

It is also demonstrated that seabird presence on islands promotes primary production on adjacent reefs, theoretically through the guano-enrichment of precipitation-driven surface runoff – a mechanism of the IME. Surface runoff is facilitated by precipitation, which in the Chagos Archipelago is largely driven by the Madden-Julian Oscillation, alongside the monsoon seasons. However this link between precipitation and nutrient influx is unproven.

The importance of addressing these knowledge gaps is that understanding the distribution of primary production forms the foundation to support a variety of further processes. Primary production can influence the health of reefs, as well as the distribution of organisms from zooplankton to apex predators. Developing our understanding of primary production drivers within the Chagos Archipelago will explain the mechanisms by which the Chagos Archipelago is a biological ‘hotspot’ in an otherwise oligotrophic ocean.

Here, we aim to address this gap in knowledge, by testing the hypotheses that:

- surface runoff from land supports elevated primary productivity within the archipelago
- upwelling from below the nutricline supports elevated primary productivity within the archipelago

therefore, determining the dominant climate and oceanographic mechanisms responsible for enhancing primary production which promotes the biodiversity and high biomass (Samoilys *et al.*, 2018) found within the archipelago, as well as providing insight into how these nutrient sources may vary spatially.

2. Methods:

2.1. Bathymetric Data:

Bathymetric data was obtained from the General Bathymetric Chart of the Oceans (GEBCO), grid version 2021 (GEBCO Compilation Group, 2021) at 15 arc-second resolution. This is a global scale gridded bathymetry chart, comprised of many regional-scale bathymetric surveys compiled into one grid.

2.2. Precipitation Data:

ERA5 precipitation data was acquired to determine when surface-runoff was facilitated. This data was obtained from the European Centre for Medium-Range Weather Forecasts (https://ecmwf.int/) at 30km resolution – a hindcast resulting from a combination of *in situ* measurements and climate modelling. From this, the daily total precipitation was calculated, for the period of time the moorings were deployed. It must be noted that the 30km scale of this model is coarse, especially when studying a particularly small land mass.

2.3. Remote Sensing:

2.3.1. Detection of Chlorophyll:

Elevations in chlorophyll-a concentration are widely used as an indicator of increased primary production. Surface chlorophyll-a concentrations can be derived from satellite ocean colour data, by using green/blue ocean colour algorithms (Ding, 1987; O'reilly *et al.*, 1998; Hu, Lee and Franz, 2012), or using solar-induced fluorescence (SIF) (Ding, 1987; Gower, 2014; Gupana *et al.*, 2021) as a proxy. There are advantages to using SIF as a proxy for chlorophyll-a concentration over ocean colour algorithms, particularly in coastal waters, as the fluorescence signal is specific to chlorophyll-a (Xing *et al.*, 2007), so it is less vulnerable to interference from suspended particulate matter and coloured dissolved organic material (Xing *et al.*, 2007; Gower, 2014), compared to green/blue algorithms. There are however some inherent physiological and optical uncertainties in the product. Algal physiology provides uncertainty as the fluorescence quantum yield varies, depending on species composition, nutrient availability, temperature and light (Abbott and Letelier, 1999). Therefore spatial and temporal variation in the fluorescence signal may be caused by a variation in the fluorescence quantum yield, rather than a change in algal concentration. Uncertainties can also arise due to bottom contamination influencing the reflected spectrum (Barnes *et al.*, 2013). Here, we use the product 'normalised fluorescence line height' (nFLH) which is a type of SIF measurement, normalised against the solar zenith angle.

The remote sensing of primary production in Chagos is complicated by the presence of a deep chlorophyll maximum (DCM, often referred to as a subsurface chlorophyll maximum) occurring at around 50/75 metres (George *et al.*, 2012, 2018; Fasolo, 2013). Light attenuation occurs in the water column, with the solar radiation (light) attenuating on the downwelling path to the phytoplankton, and fluorescence returning towards the satellite sensor being attenuated also (Gupana *et al.*, 2021; Serôdio and Campbell, 2021). This means that not only does the attenuation of light limit the depth at which chlorophyll can be detected by satellite-derived SIF, but also that chlorophyll at depth will return a weaker signal than surface chlorophyll.

The temporal resolution at which the level 3 nFLH data is available (8-daily or monthly) is too coarse to allow for the interpretation of high-frequency influences such as tides. It is however well suited for the analysis of how longer time-scale processes (i.e., the Indian Ocean Dipole) may influence localised productivity. Level 2 coverage is available at a 1-2 day resolution but cloud cover is often high, inhibiting data collection.

2.3.2. Station Selection for Evaluation of Chlorophyll Variability:

To test whether the relationship between SIF and SST varied with water column depth, 3 stations were selected along a transect at a latitude of 6°S (table 1), to encompass a large depth gradient. These stations are uniformly spaced, spanning from the shallow waters (~20m) at station 1 (henceforth 'Great Chagos Bank'), through station 2 (henceforth 'mid-water') across to station 3 in deep-water (~5400m) channel that runs along the east of the archipelago (henceforth 'deep-water'). There is also a 4th station at Egmont atoll to include the potential impact of land (henceforth referred to as 'Egmont'). Station locations are shown in figure 5.

Table 1: Station locations and depth.

STATION	LATITUDE (°N)	LONGITUDE (°E)	WATER DEPTH (M)
1	-6	72.5	20
2	-6	73.125	3000
3	-6	73.75	5380
4	-6.65	71.35	15

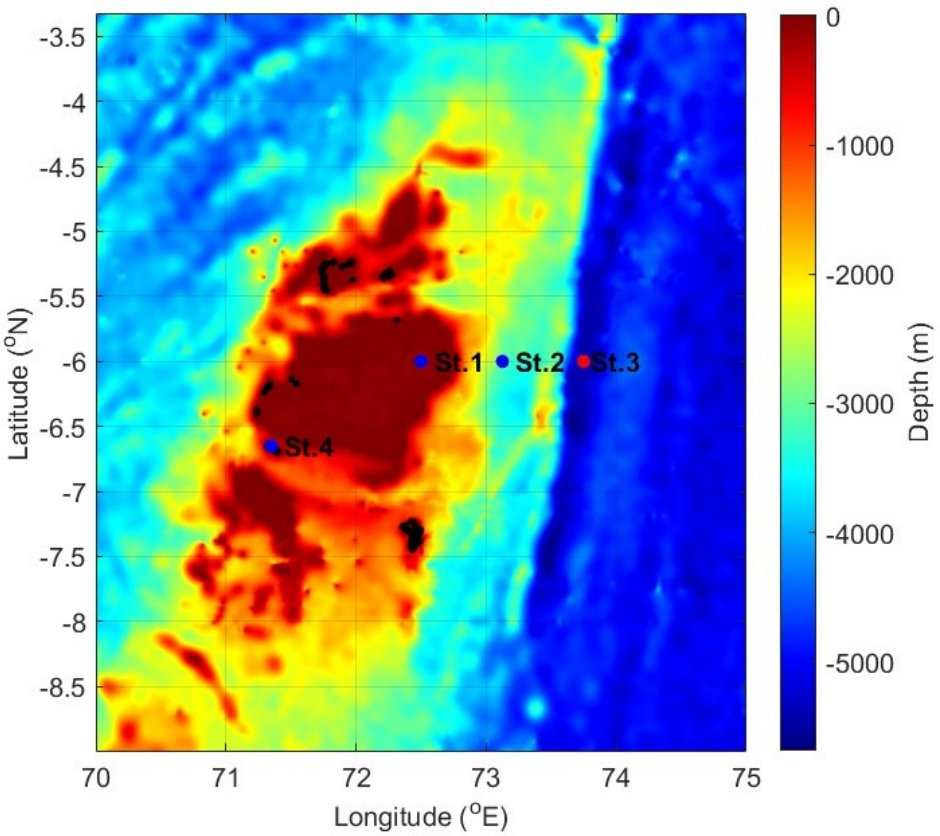

Figure 5: Bathymetric map of the Chagos Archipelago, with the four station locations marked with circles. Land masses are also outlined in black. Created using GEBCO bathymetric data.

2.3.3. Remote Sensing Products and Sources:

We used normalised fluorescence line height (nFLH) as a measure of solar induced fluorescence, a proxy for elevated primary production. Specifically, the product used was 'Normalized Fluorescence Line Height' (MODISA_L3m_FLH_v2018) collected by the NASA Moderate Resolution Imaging Spectroradiometer (MODIS)-Aqua sensor. This data was accessed via NASA's Giovanni application (http://giovanni.gsfc.nasa.gov/). This data is provided at 4km resolution as a monthly averaged value to remove the breaks in data caused by cloud cover and spans the period 04/07/2002 to 31/12/2021. This product is normalised by dividing by the cosine of the solar zenith angle. The formula for calculating nFLH is given as:

$$nflh = nLw(678) - \left(\frac{70}{81}\right) \times nLw(667) - \left(\frac{11}{81}\right) \times nLw(748)$$

calculated as the difference between the observed $nLw(678)$ (the fluorescence signal) and the linearly interpolated $nLw(678)$ from the surrounding bands $nLw(667)$ and $nLw(748)$ (Abbott and Letelier, 1999).

Sea surface temperature (SST) data was also obtained from the MODIS-Aqua sensor, via Giovanni. This is at the same spatial and temporal resolution as above. The specific product used was sea surface temperature at 11 microns (day) (MODISA_L3m_SST_Monthly_4km_vR2019.0). This data spans the period 04/07/2002 to 31/12/2021. Here, the data used was collected by the MODIS-Aqua mission, selected due to the long data set from the same sensor, and relatively fine spatial resolution.

Surface wind speed data was acquired from the MERRA-2 model, a global coverage model, via Giovanni. This was provided at a spatial resolution of 0.5 x 0.625°, at a monthly temporal resolution, from 04/07/2002 to 31/12/2021.

2.3.4. Remote Sensing Data Handling:

All data analysis was performed using MATLAB R2021b. Climatologies of SST, wind speed and nFLH were created by calculating the monthly averages at each station throughout the full 20-year data set, to show seasonal variation. From this, monthly anomaly values could also be calculated by removing this seasonal variation. Linear regression was used to assess the relationship between SST, wind speed and nFLH, as well as SST anomaly, wind speed anomaly and nFLH anomaly, at each station.

2.4. *In Situ* Observational Methods:

In surface waters at low latitudes, nitrogen limitation is the typical limiting factor for primary production (Moore *et al.*, 2013). The *in situ* measurement of nutrients allows for the direct measurement of a given nutrient (in this case nitrate, NO_3). This is a much more reliable process for the interpretation of nutrient sources compared to using remotely sensed proxies, as not only does it provide much higher spatial and temporal resolution, but it also removes many external factors associated with the remote sensing of chl-a as an indicator of nutrient variability. This does however come at the expense of spatial coverage.

The high temporal resolution of the *in situ* nitrate measurements allows for the observation of changes in nutrient concentration with much higher frequency than was possible with remote sensing. Sampling at 1-minute intervals enables the impact of tides to be resolved, as well as high frequency, short timescale impacts such as rainfall inducing surface runoff – attributed by Graham et al. (2018) as a key nutrient source.

2.4.1. Egmont Atoll Mooring Locations:

The study site was on the northern side of Egmont Atoll (within the bounds of station 4), in the lagoon inlet as shown in figure 6. Here, water depth was approximately 6m. Previous studies at this site have indicated that this region is subjected to processes resulting from lagoon outflow (Harris *et al.*, 2021), making it well suited for assessing the possible impact of surface runoff, where water exiting the lagoon would be directed past the instruments on the ebb tide.

Figure 6: A satellite view of the Egmont Islands, with the location of the CTD, nitrate sensor and ADCP marked. Image © 2023 Maxar Technologies (Google Earth Pro 7.3.3, 2022).

2.4.2. *In Situ* Instrumentation:

Moorings were deployed at this site on 14th March 2022. The moorings consisted of an RBR Concerto conductivity-temperature-depth (CTD) sensor sampling at 2-second intervals, a TriOS OPUS UV spectral sensor (nitrate sensor), sampling at 1-minute intervals, and a Nortek Eco ADCP, sampling at 2-minute intervals. These sampling rates were the highest that was possible for each instrument with the storage capacity and power supply available, as the data was for use by a multi-disciplinary team, and averaging/binning was possible in post-processing. The moorings were then recovered on 30th March 2022, for a total sampling period of 17 days. A second CTD, an RBR Maestro, was also used for profiling at multiple locations throughout the cruise. To handle the different response times of the sensors, the profiling instruments were hand-deployed at a sufficiently slow speed to allow the instrument to operate correctly.

2.4.3. *In Situ* Data Handling:

The data analysis and production of figures were performed using MATLAB R2022a, however some pre-processing was necessary for the CTD data, using the software 'Ruskin v2.19.1.202210211844' as provided by the CTD manufacturer RBR. To account for the difference in sampling rates between the OPUS and the RBR Concerto, the data collected by the CTD was averaged into 1-minute bins centred on the times the OPUS sampled at – both removing high-frequency noise as well as allowing for better comparison between the data sets. Data corresponding to either an ebb or flood tide were separated by applying a Savitzky-Golay filter (polynomial order = 3, frame length = 401) to the depth recorded by the CTD (this was to remove wave noise and keep the tidal signal); then calculating the gradient of this data where a positive value meant increasing water depth (flood tide) and a negative gradient meant decreasing water depth (ebb tide). As the data were time-synchronous, other variables such as temperature or nitrate concentration could then be extracted for either the ebb or flood tide. The data was tested for normality using the Jarque-Bera test, where the null hypothesis that the data were normally distributed was rejected at the 0.05 significance level. Mann-Whitney u tests were performed to test for significance in difference between the ebb and flood tides, according to the formula:

$$\boldsymbol{U_1 = R_1 - \frac{n_1(n_1 + 1)}{2}}$$

or

$$\boldsymbol{U_2 = R_2 - \frac{n_2(n_2 + 1)}{2}}$$

where U is the smaller of U_1 and U_2, R_1 is the sum of ranks in sample 1, R_2 is the sum of ranks in sample 2, n_1 is the number of items in sample 1 and n_2 is the number of items in sample 2.

Results:

3.1. Regional Spatio-temporal Chlorophyll-a Distributions:

Satellite data revealed that higher nFLH and cooler water was found around land, and above shallow water bathymetric features such as Great Chagos Bank (Figure 7). Across all 4 stations, it was observed that an increase in SST was associated with a decrease in nFLH (figure 8). SST variation across the 4 stations remained relatively similar at any given point in time, with the monthly averages across the stations varying by <0.5°C, and annual mean SST closely grouped (table 2). There was also no permanent temperature gradient across the 4 stations. Monthly averages of nFLH varied by a greater magnitude, with Great Chagos

Bank having a monthly average consistently higher than all stations other than Egmont year-round. The annual mean at Great Chagos Bank was 27% higher than at the deep-water station.

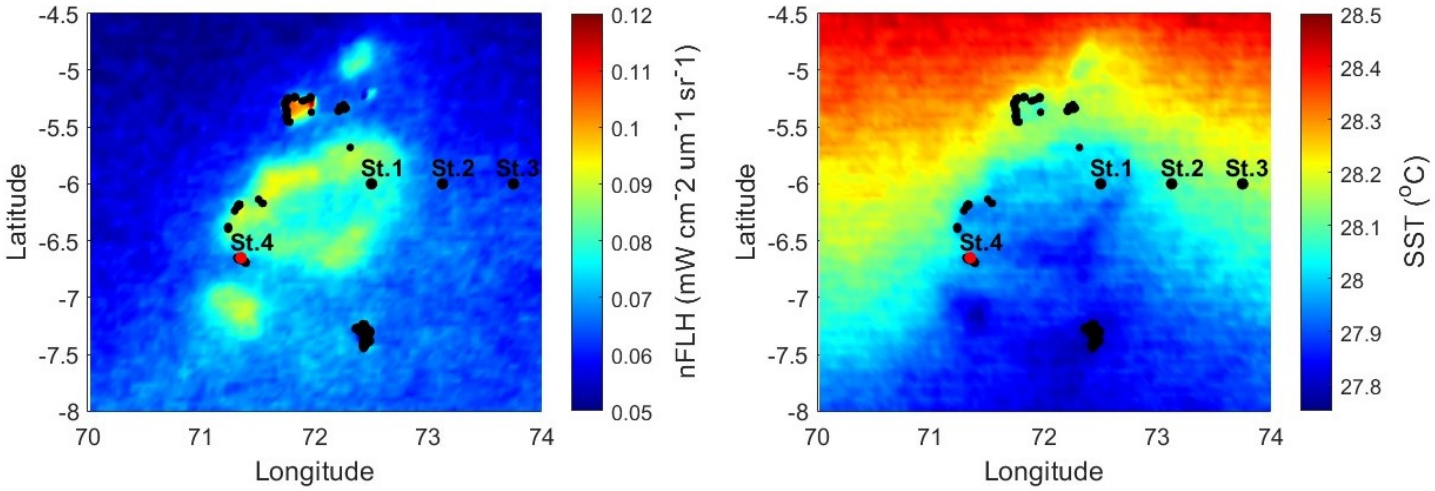

Figure 7: Left: normalised fluorescence line height, time averaged from 04/07/2002 to 31/12/2021. Right: sea surface temperature, time averaged from 04/07/2002 to 31/12/2021. Latitude and longitude shown as °N and °E. Land masses are shown in black.

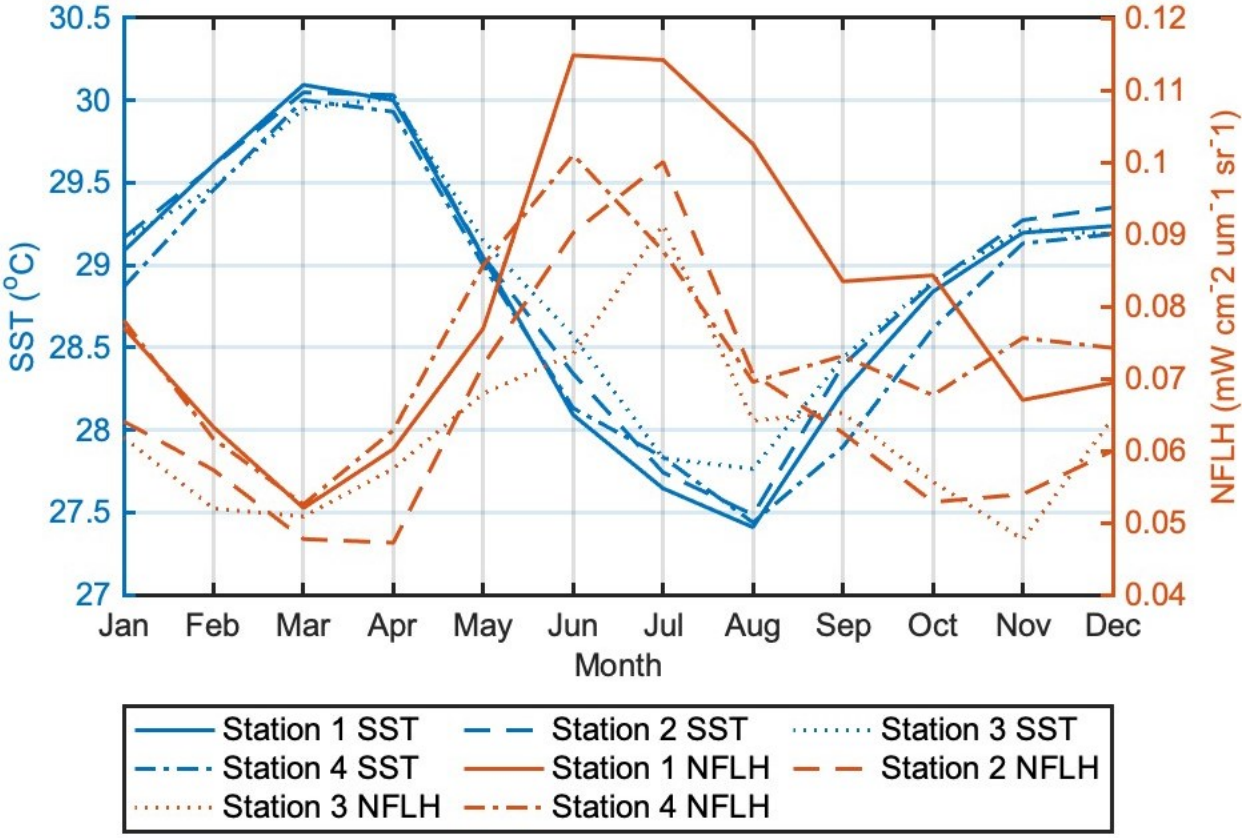

Figure 8: Climatologies of SST and NFLH at the 4 selected stations.

Table 2: Annual mean SST and nFLH at each station

STATION	ANNUAL MEAN SST (°C)	ANNUAL MEAN NFLH ($mW\ cm^{-2}\ \mu m^{-1}\ sr^{-1}$)
1	28.87	0.080
2	28.95	0.065
3	28.97	0.063
4	28.79	0.074

Linear regression was performed to test whether SST significantly predicted nFLH across the stations (Table 3, Figure 9). At all stations, SST significantly predicted nFLH (p=<0.001) although the explanatory power was low, and that SST anomaly significantly predicted nFLH (p=<0.001). In the case of SST and nFLH as well as of the anomaly data, the R^2 was highest at station 1 over Great Chagos Bank, and comparatively weak at stations 2, 3 and 4. A statistically significant relationship between wind speed and nFLH was found using linear regression across all 4 stations (p = <0.001) (Table 3, Figure 10), but wind speed anomaly only significantly predicted nFLH anomaly at station 1 (p = 0.04).

Table 3: Linear regression output

VARIABLES	STATION	SLOPE	INTERCEPT	R^2	P-VALUE
SST AND NFLH	1	-0.02	0.659	0.39	<0.001
	2	-0.013	0.451	0.19	<0.001
	3	-0.013	0.449	0.17	<0.001
	4	-0.011	0.381	0.13	<0.001
SST ANOM.	1	-0.017	0.000	0.18	<0.001
AND NFLH	2	-0.010	0.000	0.07	<0.001
ANOM.	3	-0.014	0.000	0.10	<0.001
	4	-0.012	0.000	0.08	<0.001
WIND SPEED	1	0.012	0.010	0.22	<0.001
AND NFLH	2	0.007	0.019	0.11	<0.001
	3	0.006	0.028	0.06	<0.001
	4	0.005	0.045	0.06	<0.001
WIND SPEED	1	0.005	0.000	0.02	0.04
ANOMALY	2	0.001	0.000	0.00	0.44
AND NFLH	3	0.002	0.000	0.00	0.349
ANOMALY	4	0.003	0.000	0.01	0.166

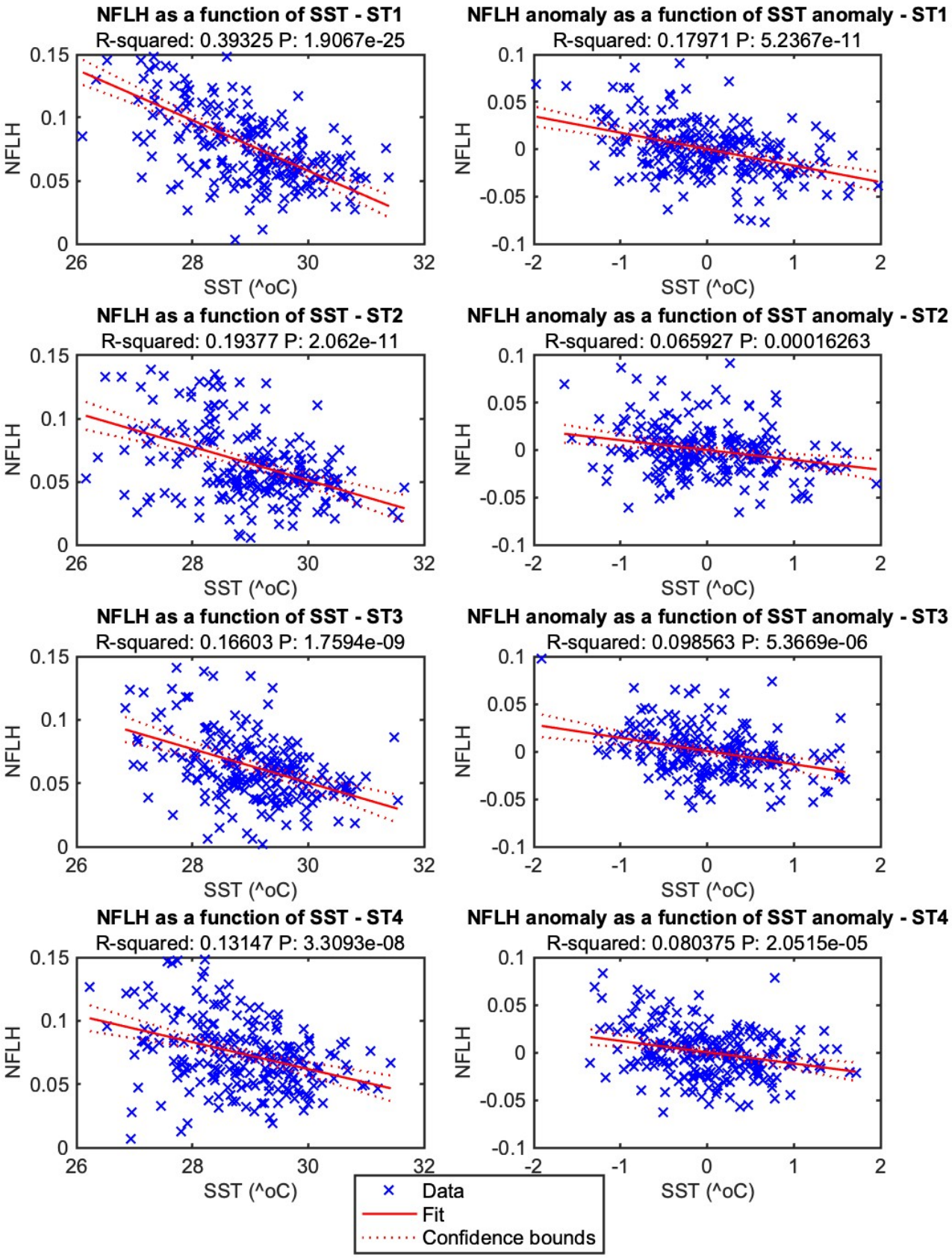

Figure 9: Linear regression analysis of the relationship between SST and nFLH. Left column: analysis of values of nFLH as a function of SST. Right column: analysis of nFLH anomaly as a function of SST anomaly.

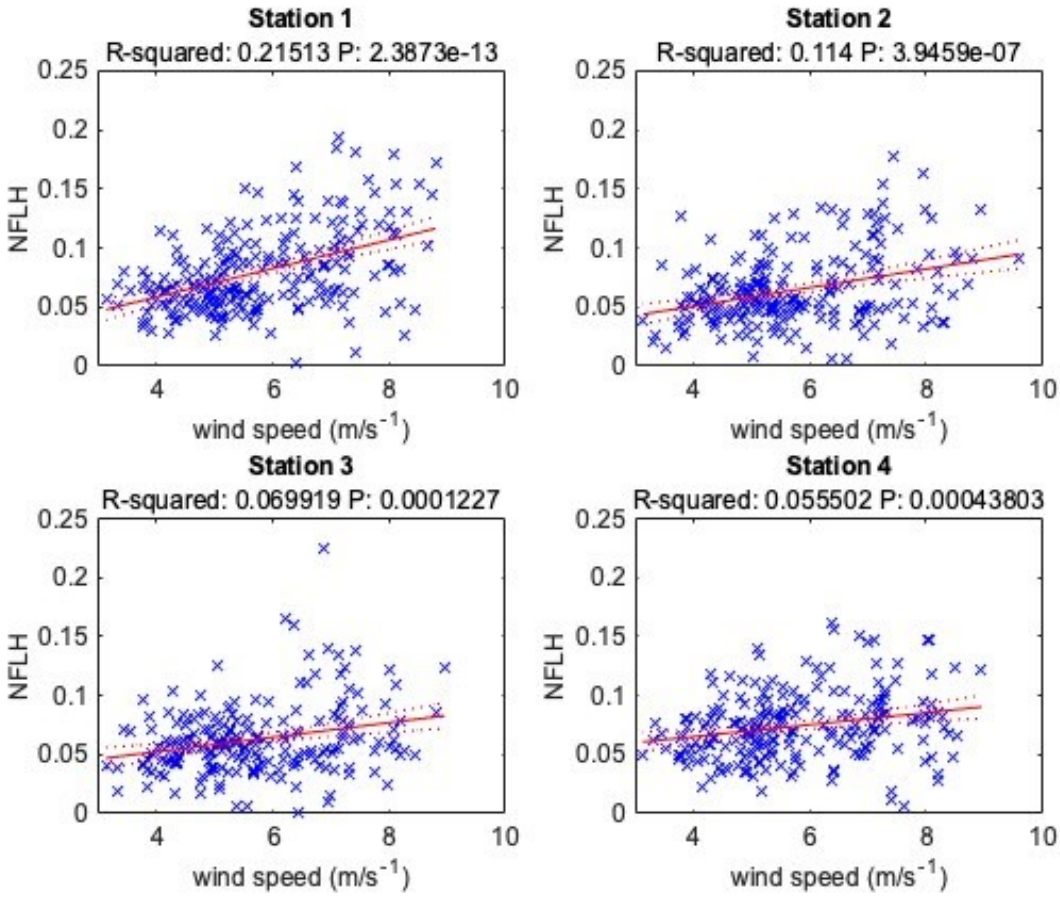

Figure 10: Linear regression of nFLH as a function of wind speed.

3.2. Local Temporal Nitrate Distributions and Corresponding Drivers:

3.2.1. Influence of Local Stratification:

The fixed position of the mooring allows for the examination of temporally changing conditions at a given location, and interpretation of what processes elevate nutrients at the mooring site. The CTD profiles provide insight into the vertical distribution of water properties, allowing for interpretation of the source of changes at the mooring.

CTD profiles throughout the region revealed a surface mixed layer, with a thermocline beginning at approximately 30-45m and a halocline beginning at approximately 12-20m in March 2022 (figure 11), showing a strong stratification at the base of the surface mixed layer. Surface salinity and temperature was relatively uniform across all stations, with a surface temperature of ~29°C and salinity of ~33.7 PSU. Figure 11 depicts 13 separate CTD profiles, collected at a variety of locations within the Chagos Archipelago, intended to depict the vertical distribution of temperature and salinity throughout the cruise.

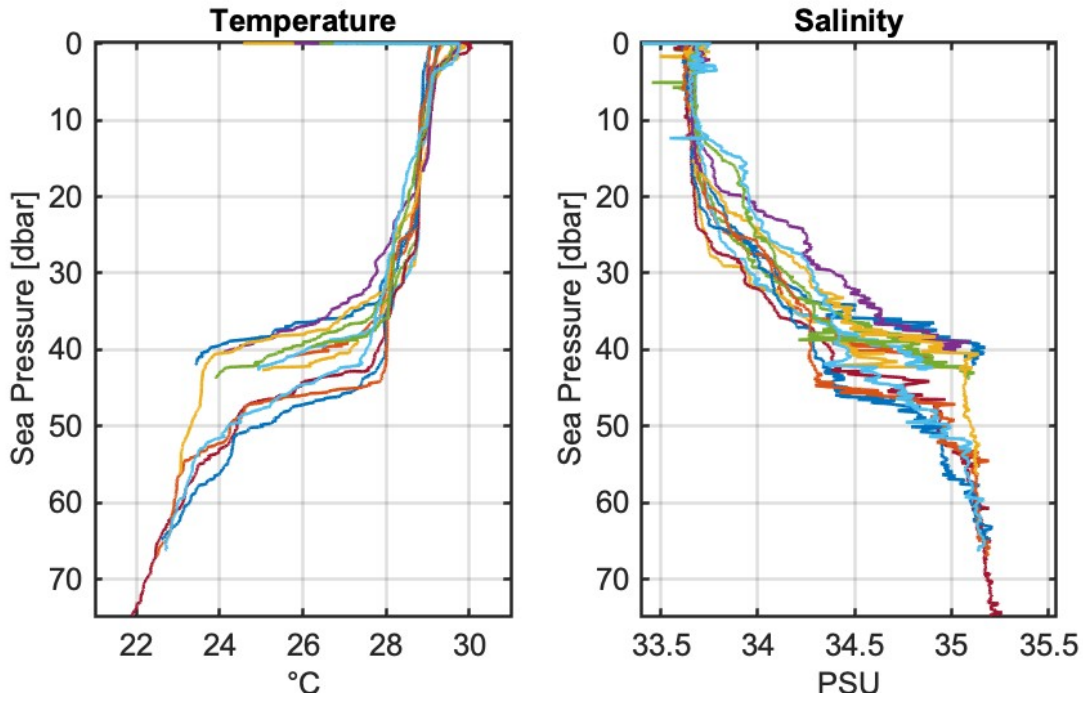

Figure 11: Temperature (left) and salinity (right) profiles from multiple locations throughout the Chagos Archipelago, during the March 2022 cruise. Note that profiles do not represent a change at a given location, but rather encompass the variability throughout the region during the mooring deployment.

3.2.2. Tidal Variability:

With the ebb and flood tidal phases separated from the moored CTD, a difference in water properties was observed between the ebb and flood tides. The mean flood phase was found to be both cooler (by 0.07°C) and more saline (by 0.025 PSU) than the ebb (figure 12).

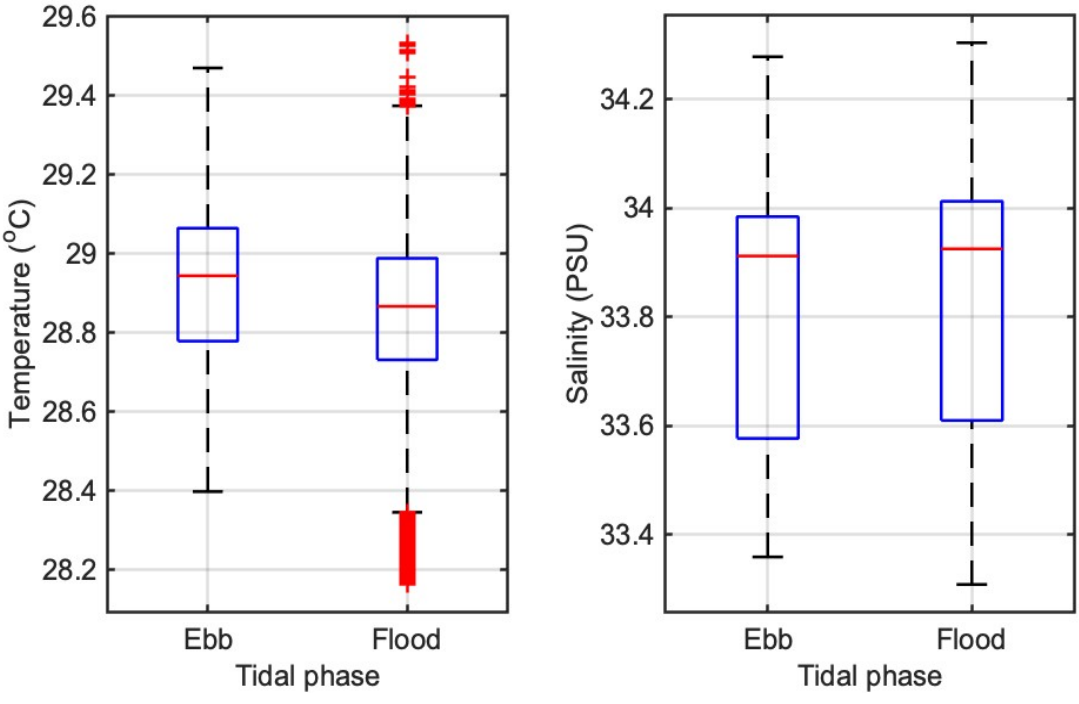

Figure 12: Comparison box plots of temperature (left) and salinity (right) on ebb and flood tides.

A semi-diurnal tide is experienced here, as shown in figure 13. Mann-Whitney U tests were performed to compare the temperature, salinity and nitrate concentration on the ebb and flood tides, to test for a difference in water properties between the tidal phases. The alpha was set to 0.05 for each test, and as three separate tests were being performed, a Bonferroni correction was applied to the so that $\alpha_{corrected}$=0.05/3 or 0.0167. There was a significant difference in temperature between ebb tide (M = 28.9258°C, SD = 0.1762) and flood tide (M = 28.8516°C, SD = 0.1792); U = -30.301, p = <0.001, and a significant difference in salinity between ebb tide (M = 33.8210, SD = 0.2155) and flood tide (M = 33.8457, SD = 0.2209); U = 9.809, p = <0.001. Both these results remain significant after Bonferroni correction. However, there was not a significant difference in NO_3 between ebb tide (M = 0.5312, SD = 0.0929) and flood tide (M = 0.5299, SD = 0.1076); U = 0.078, p = 0.938.

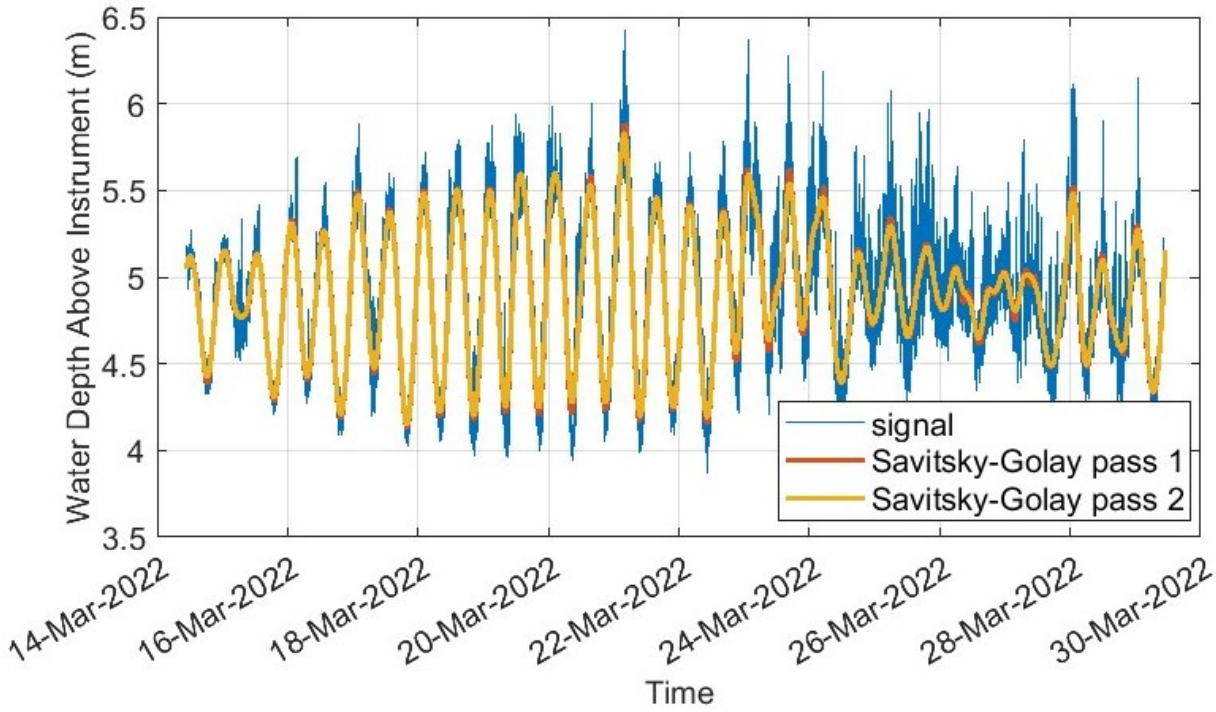

Figure 13: Tidal curve showing water depth above the CTD, before and after savitsky-golay filtering to remove wave noise.

The ADCP situated in the entrance to Egmont lagoon provided insight into the flow patterns experienced here. Despite the movement of water in and out of the lagoon on the ebb and flood tide, the dominant flow direction was in line with the deep-water channel between Egmont and Great Chagos Bank (Figure 14). The data shown is averaged across the middle 2m depth bin (2-4m depth) however the flow measured here was vertically homogenous. On the ebb tide there was very little movement detected in a south-easterly or north-westerly direction, which would be indicative of a current flowing into or out of the lagoon. However, on the flood tide there was flow detected in a south-westerly direction, evidence of water flowing in through the lagoon mouth. This would be indicative of water being carried past

the moorings from outside the atoll, where it can also be detected by the CTD and nitrate sensor.

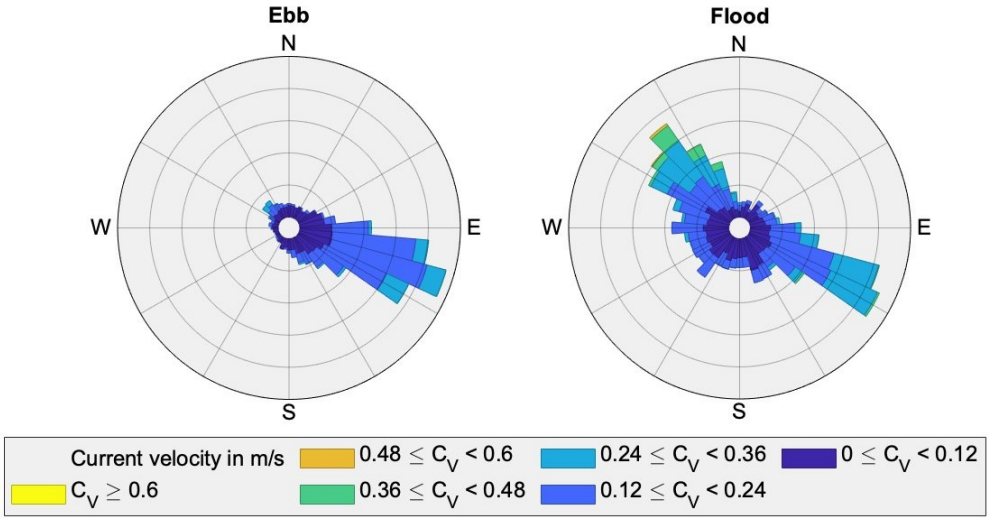

Figure 14: ADCP data showing flow direction and intensity from the mouth of Egmont lagoon, separated by ebb and flood tidal phases.

3.2.3. Temporal Nitrate Variability:

ERA5 precipitation data shows daily total precipitation to decrease from 7mm to 0mm in the first 4 days, rising back to an average approximately 2mm/day, with a 2-day peak on March 23rd (11mm) and 24th (9mm). NO_3 concentrations from the mooring show a similar pattern, with an approximately 2-day lag (figure 15), where NO_3 peaks at 0.64 on March 26th, 2 days after the precipitation peak. The speed of this response shows that the time it takes for groundwater to enter the atoll, plus the residence time of the atoll, totals approximately 2 days.

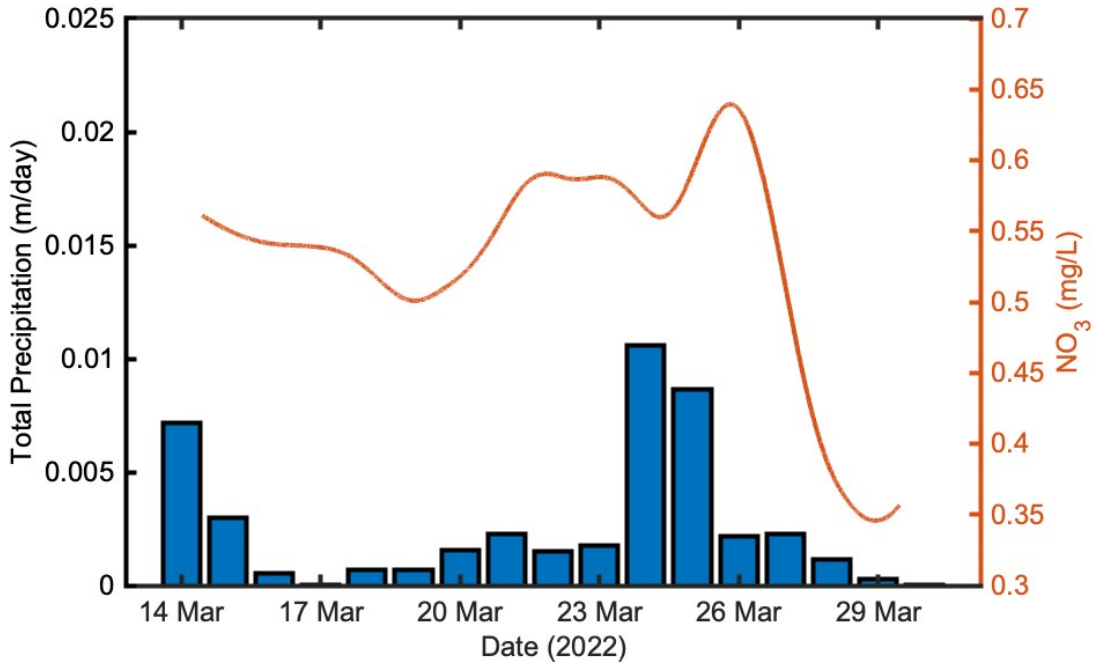

Figure 15: Time series of daily total precipitation and NO_3 concentration

It is evident from the CTD and nitrate data that the peak in nitrate occurred at the same time as the freshening of the water, driven by the precipitation (figure 16). Prior to March 24th (when precipitation peaked) the average salinity was 33.98 PSU. This decreased to 33.57 PSU after the precipitation peak. Nitrate concentration began to increase on the 24th at the same time as the freshening, peaking at 0.64 mg/L 48 hours later, which was an increase of 21% above the average nitrate concentration for the mooring period. As salinity decreases, there is more noise in the data. This can likely be attributed to the fact that an optical sensor was used, and the surface runoff will have increased turbidity, introducing noise caused by particulate organic matter.

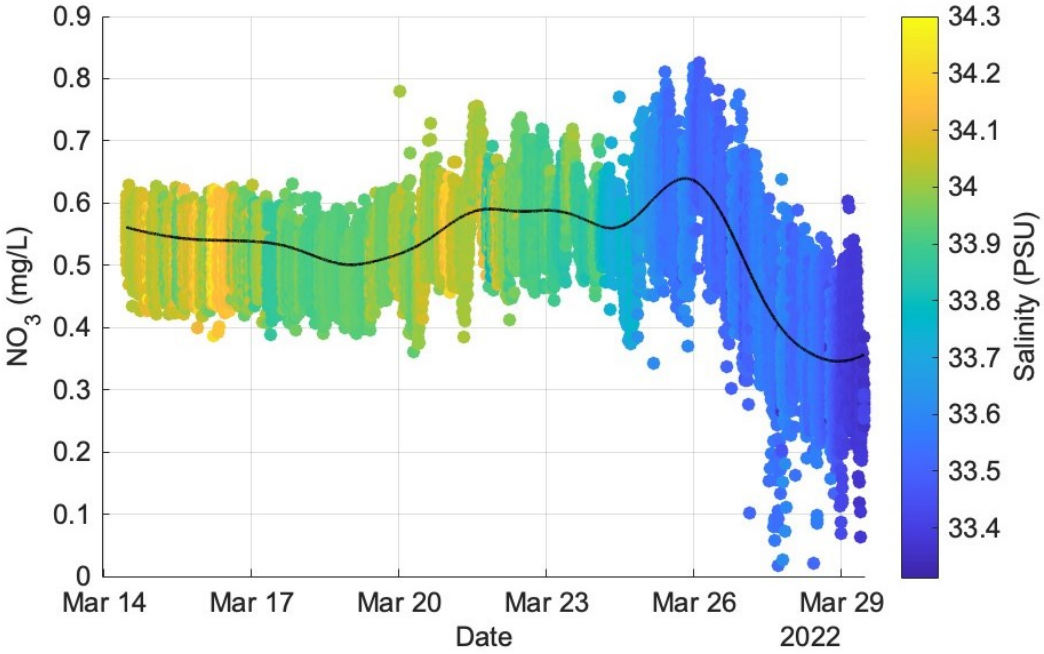

Figure 16: Time series of NO_3 concentration, where point colour represents salinity. Black line depicts smoothed NO_3 data.

4. Discussion:

4.1. Regional Distribution of Chlorophyll as a Proxy for Primary Production:

There is an apparent correlation between water depth and surface nFLH, with shallower regions appearing to have a higher nFLH. This observation is supported by the nFLH climatology of each station (figure 8) which showed that across the stations away from land (1,2 and 3), average nFLH for any given month was strongest at Great Chagos Bank, decreasing as depth increased through stations 2 and 3. The exception to this was Egmont, which fluctuated and did not follow the same pattern. This would suggest that there are different controlling factors of chlorophyll concentration in open waters and those adjacent to land. However, this may also be a factor of remote sensing, with a shoaling of the mixed layer trapping phytoplankton nearer the surface, within the depth range of satellite sensing,

and appearing as an elevation in chlorophyll concentration identified by a higher nFLH. Alternatively, it could be caused by the influence of bottom contamination at the shallow land-adjacent station.

The annual mean nFLH was also shown to increase as depth decreased, with the annual mean at Great Chagos Bank 27% higher than that in the deep-water station. This is demonstrative of an enhancement of surface primary productivity in shallower waters, consistent with the findings of Fasolo (2013). However, again Egmont did not fit this pattern, suggesting that the presence of land in very close proximity to Egmont may be a contributing factor to the nFLH at this location.

The statistically significant relationship between SST and nFLH across all stations demonstrates that, on a seasonal scale, SST can predict nFLH. However, this relationship is stronger at station 1 (R^2=0.39) than stations 2, 3 and 4 (R^2 = 0.19, 0.17 and 0.13 respectively). A similar trend was seen in the relationship between SST anomaly and nFLH anomaly, with a stronger relationship experienced at station 1 (R^2 = 0.18) than at the other stations (R^2 = 0.07–0.010). This demonstrates that deviation from the seasonal average SST is often met by a corresponding deviation from the seasonal average nFLH. There was very little variation in SST between the stations, with the annual mean across the three stations all within 0.18°C, suggesting that it is not a change in SST across the stations governing the change in nFLH, but rather a change in the response to temperature change across the stations. This indicates that, in the absence of land, shallower waters may be more sensitive to stratification (for example by preventing shear-induced turbulent mixing across the thermocline), consequently limiting primary productivity by limiting nutrient entrainment.

The statistically significant relationship between surface wind speed and nFLH is also indicative of wind being a controlling factor behind the seasonal variation of primary productivity, a phenomenon which has been observed elsewhere (Zhang *et al.*, 2014; Shen *et al.*, 2018; Chen *et al.*, 2020). However, the lack of significant relationship between wind speed anomaly and nFLH anomaly is not consistent with previous studies (e.g., Zhang et al., 2014; Chen et al., 2020). This may be an artefact of the limitations of remote sensing in detecting subsurface chlorophyll, rather than a true reflection of the relationship between elevated wind speeds and the enhancement of primary productivity.

There are many mechanisms by which the impact of wind speed and SST may be amplified in shallower waters. The SML depth in Chagos is typically between 25 and 50m (Vissa, Satyanarayana and Prasad Kumar, 2013). Under these conditions, in the shallow waters above Great Chagos Bank (station 1) where depths can be as little as 6m, the SML will likely span the full water column. Under these conditions, processes by which nutrients could be entrained from below the SML (such as shear instability) are not possible. Elevations in wind speed may also drive processes in the shallower waters which are not present at the deeper stations. Wind-driven turbulent mixing in the surface mixed layer can trigger the resuspension of detritus into the water column (Chen *et al.*, 2010), which may provide a nutrient source (Sloth *et al.*, 1996) localised to the shallower waters where the SML and seabed interact.

The presence of a DCM in Chagos (George *et al.*, 2012, 2018; Fasolo, 2013) means that satellite-derived measures of chlorophyll-a (both ocean colour and SIF) should only be used as an indication of surface primary production, and not a measure of total primary productivity at a given location. Although the relationship between wind speed and nFLH appears stronger in shallower water, elevation in wind speeds can deepen the MLD. If the subsurface chlorophyll maximum occurs at the base of the mixed layer, this deepening of the SML may entrain more nutrients, and enhance productivity, but also deepen the depth at which it occurs. Due to the additional attenuation of light because of the deepening (Gupana *et al.*, 2021; Serôdio and Campbell, 2021), satellite data would not show this enhancement to its full extent. To analyse this relationship more reliably, the collection *in situ* fluorescence profiles to compare with satellite values would be beneficial.

Both SST and nFLH data are provided at 4x4km spatial resolution. At this pixel size, it is possible to distinguish features between the three stations, as they are all separated by a minimum of ~70km, so the averaging across the pixel will not cause overlap between the stations. The monthly temporal resolution allows for the observation of seasonal variation but is too coarse to isolate impacts of short timescale events occurring on a scale of weeks, such as the Madden-Julian oscillation (Webber *et al.*, 2014), which operates on an approximately monthly cycle. Data averaging across each month will have removed any artefacts occurring on a fine scale (e.g., shorter than monthly).

It is important to note that the normalisation of the fluorescence data has been found to mask some features, and boost others. This normalisation is performed to correct the data

to compensate for solar zenith angle, which contributes to the seasonal cycle present in the data (Gower, 2014). This is a limitation of this study, and a repeat of the analysis with the fluorescence data pre-normalisation would be beneficial. NASA do not currently publish their fluorescence line height data without this normalisation applied.

4.2. Local-Scale Mechanisms Driving Nutrient Availability:

CTD profiles revealed a steep thermocline and halocline at approximately 40-50m, providing evidence of a highly stratified environment. Under these conditions, it takes a lot of energy to overcome this stratification and allow the vertical transport of water into the surface mixed layer. The flood tides were cooler and more saline than the ebb tides (figure 12), and the water from below the thermocline was also cooler (by approx. 6°C) and more saline (by approx. 1.5 PSU) (figure 11). This represents a shift in temperature and salinity at the mooring towards those found below the thermocline, supporting the theory that the flood tide may be promoting mixing across the base of the surface mixed layer, transporting cooler deep water into the SML. However, this deep water would also typically be expected to be higher in nitrate, as the Indian Ocean often experiences a nitracline at the pycnocline depth (Resplandy *et al.*, 2009); but there was found to be no significant difference in nitrate between the two tides. This would therefore suggest that deep water entrainment is playing little role in the governing of surface nitrate concentration on this temporal scale.

It is important to note that although the shift in temperature and salinity towards those from below the thermocline was experienced on the flood tide, it is entirely possible that this tidally driven mixing is occurring on the ebb tide too, but not reflected in the data due to the location of the mooring. As shown by the ADCP data at Egmont (Figure 14), the dominant current ran parallel to the outer edge of the atoll, following the depth contour on both the ebb and flood tidal phases, but there was also a signal showing flow in a south-westerly direction on the flood tide only. This current will have been moving from the deep waters outside the lagoon, up the atoll slope into the lagoon through the narrow channel, and will have directed flow from the deeper waters past the CTD sensor, which would explain the cooler and more saline flood tide recorded at the moored CTD.

Prior to the mooring deployment, there had been a period of approximately 10 days of rainfall, ending the day before the nitrate sensor and CTD were moored. Under these conditions, surface runoff will have been present, likely increasing the nitrate concentration in the water. This means that when the instruments began recording, there will have been

an elevated background nitrate concentration. A peak in precipitation occurred on March 24th, which led to a decrease in salinity, corresponding with a peak in nitrate. The correlation between the timing of the freshening and increase in nitrate suggests that it is the fresh water resulting from precipitation carrying nitrate from land with it. This aligns with previous findings in Chagos (e.g., Graham et al., 2018), with the leaching of land-based nutrients such as seabird guano being a key nutrient source. There is also significance to the drop in nitrate concentration following the rainfall and nutrient peak; the nutrient source on land accumulates over time as a result of guano deposition, and once this source is depleted, continued rainfall would have a reduced effect. The drop in nitrate is likely to be due to the fact that the accumulated guano had been transported into the lagoon, and nutrient leaching was greatly decreased. It could be theorised that the longer the period between rainfall events, the more guano would accumulate, increasing the amplitude of the nutrient influx when rainfall did occur – however this would require data collection over a longer period to test reliably.

Despite the presence of invasive rats on the islands of Egmont, high numbers of seabirds were experienced on land and in the skies above them during the cruise. These findings demonstrate that whilst rat-infested islands experience far lower seabird densities (Graham *et al.*, 2018; Benkwitt, Wilson and Graham, 2019), land based nutrient leaching in Chagos remains an important source of nutrients even in the presence of rats. It would be expected that on the rat-free islands, the increased seabird densities and nitrogen deposition rate reported by Graham et al. (Graham *et al.*, 2018) would lead to an amplified nutrient input caused by rainfall.

According to the NOAA Dipole Mode Index, the DMI was in its negative phase during the time the moorings were deployed, with a strength of -0.093. This will have led to a decreased SST and weakened stratification as a result, as well as an enhancement of SCTR upwelling due to atmospheric forcing. This will have led to an elevated level of nutrient upwelling regionally, resulting in a higher background nitrate concentration.

With the knowledge that rainfall drives an elevation in nitrate in the waters surrounding land, in can be inferred that climate oscillations that bring precipitation will lead to increased nutrient availability. The Madden-Julian oscillation passes at regular intervals, of 30-60 days, and therefore can be viewed as a regular driver of nutrient input. The Indian Ocean Dipole however operates on a far longer timescale (approximately annual) and does not follow a

regular pattern. It is projected that as a product of climate change, positive IOD phases will become more frequent and more extreme (Cai *et al.*, 2021). Whilst this would suppress SCTR upwelling, it would also cause increased rainfall, potentially increasing land-based nutrient runoff. However, with the globally increasing stratification discussed by Sallée et al. (Sallée et al., 2021), it could be expected that seabird nutrition would decrease also, further limiting the nutrient supply in the form of seabird guano as well as restriction upwelling from below the thermocline.

It is important to consider that whilst remote sensing relies on the remotely sensed chlorophyll as an indicator of where nutrient levels were likely enhanced, here we present direct measurements of nitrate. Whilst nitrate is utilised by phytoplankton in primary production, this process is not instantaneous, so nitrate will be carried away from the mooring location by tides/currents before photosynthesis occurs, meaning that it could be reflected in remote sensing data at a different location. This is of particular relevance to small-scale nutrient input, which can be quickly dissipated before it could be reflected in remote-sensing data. This would mean that there would be a local impact for organisms which benefit from nitrate directly (such as coral), but for those which benefit from phytoplankton, the local enhancement will have dissipated.

5. Conclusions:

Both SST and surface wind speed were found to be significant predictors of nFLH across all stations ($p = <0.001$). SST exhibits a negative correlation with nFLH, and wind speed exhibits a positive correlation. SST and surface wind speed both relate to the impact of stratification, with elevated SST being associated with increased stratification, and elevated wind speeds promoting turbulence that may overcome this stratification to allow vertical mixing. This suggests that in shallower water and in the absence of land, the strength of stratification plays a more critical role in governing primary productivity. The fact that the station at Egmont atoll does not follow the same pattern as the open water stations that different processes may be present as a result of this land – and therefore open water productivity may be governed by different processes than in waters immediately adjacent to land masses.

There are some inherent issues in the remote sensing of primary productivity, particularly in regions where deep chlorophyll maxima are present, where chlorophyll at depth returns a weaker signal/is not detectable. Because of this, there is the possibility that the apparent

lack of relationship between surface wind speed anomaly and nFLH anomaly is in fact a result of primary productivity occurring deeper when elevated winds deepen the SML, and further research incorporating *in situ* fluorescence profiles would be beneficial.

Whilst *in situ* evidence (in the form of moored CTD data) suggesting tidally driven mixing across the thermocline was found, there was no evidence that this process was contributing to nitrate concentration in the surface mixed layer. However, a relationship was found between precipitation and nitrate concentration, showing that rainfall-induced surface runoff, likely enriched by seabird guano, leads to elevations in nitrate. At the study site of Egmont, this was experienced with a 2-day lag between precipitation peak and corresponding nitrate peak. This agrees with existing studies supporting surface runoff as a nutrient source, and proves the value of this process, even in the presence of invasive rats which reduce seabird density.

Based on this, it can be expected that the Madden-Julian oscillation will promote primary productivity by enhancing nitrate concentrations as it passes over Chagos due to the rainfall it brings. The Indian Dipole in its positive phase will also promote elevated rainfall, leading to nitrate enhancement. Increasingly frequent and extreme positive phases of the IOD as a result of climate change will potentially lead to an increase in nitrate input.

It is apparent that in this instance, remote sensing data and *in situ* measurements indicate a different dominant nutrient source. Remote-sensed solar-induced fluorescence shows that moth SST and surface wind speed significantly influence nFLH. The strength of this relationship varies with water depth, and the presence of land also alters this relationship. These findings suggest that deep-water entrainment from below the thermocline is a key driver of nutrient concentration.

However, *in situ* measurements revealed that whilst there was evidence of tidally driven mixing, there was no related change in nitrate concentration, suggesting that deep-water nutrient entrainment may not be a dominant nutrient source in close proximity to land. Instead, precipitation was found to induce an increase in nitrate through surface runoff, with a 48-hour lag between precipitation and consequent nitrate peak, and the nitrate elevation occurring at the same time as freshening. This indicates that the nitrate is carried into the surface waters by the fresh water that fell onto adjacent land.

It must be noted that the two data sets are given at differing temporal resolution, and collected over different periods of time. The *in situ* data is at high (1-minute) temporal resolution, but only covers a period of 17 days. It is therefore well suited to observing the influence of high-frequency changes such as within tidal cycles but is not sufficiently long to observe seasonal variation. In contrast, the remote sensing data is at monthly temporal resolution, but covers 19 years. This makes it impossible to resolve high-frequency change such as tidal cycles but is well suited to analysing seasonal variation. It is therefore plausible that on a seasonal scale, nutrient availability is governed by stratification and upwelling strength, with high-frequency fluctuations being driven by land-based nutrient input.

6. Bibliography:

Abbott, M.R. and Letelier, R.M. (1999) 'Algorithm Theoretical Basis Document Chlorophyll Fluorescence (MODIS product number 20)', *NASA (http://www.modis.gsfc.nasa.gov/data/atbd)* [Preprint].

Anderson, R.C., Adam, M.S. and Goes, J.I. (2011) 'From Monsoons to mantas: Seasonal Distribution of Manta Alfredi in the Maldives', *Fisheries Oceanography*, 20(2), pp. 104–113. doi:10.1111/j.1365-2419.2011.00571.x.

Barnes, B.B., Hu, C., Schaeffer, B.A., *et al.* (2013) 'MODIS-derived spatiotemporal water clarity patterns in optically shallow Florida Keys waters: A new approach to remove bottom contamination', *Remote Sensing of Environment*, 134, pp. 377–391. doi:10.1016/J.RSE.2013.03.016.

Benkwitt, C.E., Wilson, S.K. and Graham, N.A.J. (2019) 'Seabird nutrient subsidies alter patterns of algal abundance and fish biomass on coral reefs following a bleaching event', *Global Change Biology*, 25(8). doi:10.1111/gcb.14643.

Cai, W., Wang, G., Li, Z., *et al.* (2021) 'Response of the positive Indian Ocean dipole to climate change and impact on Indian summer monsoon rainfall', in *Indian Summer Monsoon Variability*. Elsevier, pp. 413–432. doi:10.1016/B978-0-12-822402-1.00010-7.

Carranza, M.M. and Gille, S.T. (2015) 'Southern Ocean wind-driven entrainment enhances satellite chlorophyll-a through the summer', *Journal of Geophysical Research: Oceans*, 120(1), pp. 304–323. doi:10.1002/2014JC010203.

Chagos Conservation Trust (no date) *Chagos Information Portal*, *chagosinformationportal.org*. Available at: https://chagosinformationportal.org (Accessed: 17 January 2022).

Chen, M., Pattiaratchi, C.B., Ghadouani, A., *et al.* (2020) 'Influence of Storm Events on Chlorophyll Distribution Along the Oligotrophic Continental Shelf Off South-Western Australia', *Frontiers in Marine Science*, 7, p. 287. doi:10.3389/FMARS.2020.00287/BIBTEX.

Chen, Z., Hu, C., Muller-Karger, F.E., *et al.* (2010) 'Short-term variability of suspended sediment and phytoplankton in Tampa Bay, Florida: Observations from a coastal oceanographic tower and ocean color satellites', *Estuarine, Coastal and Shelf Science*, 89(1), pp. 62–72. doi:10.1016/J.ECSS.2010.05.014.

Cornec, M., Claustre, H., Mignot, A., *et al.* (2021) 'Deep Chlorophyll Maxima in the Global Ocean: Occurrences, Drivers and Characteristics', *Global Biogeochemical Cycles*, 35(4). doi:10.1029/2020gb006759.

Dave, A.C. and Lozier, M.S. (2010) ‘Local stratification control of marine productivity in the subtropical North Pacific’, *Journal of Geophysical Research: Oceans*, 115(C12). doi:10.1029/2010JC006507.

Ding, Y. (1987) ‘Observation of ocean color and fluorescence for primary production studies’, *Advances in Space Research*, 7(2), pp. 111–115. doi:10.1016/0273-1177(87)90173-6.

Doty, M.S. and Oguri, M. (1956) ‘The Island Mass Effect’, *ICES Journal of Marine Science*, 22(1), pp. 33–37. doi:10.1093/icesjms/22.1.33.

Dunstan, P.K., Foster, S.D., King, E., *et al.* (2018) ‘Global patterns of change and variation in sea surface temperature and chlorophyll a’, *Scientific Reports 2018 8:1*, 8(1), pp. 1–9. doi:10.1038/s41598-018-33057-y.

Fasolo, L. (2013) *A Baseline Study of the Oceanography of the Chagos Archipelago*. Available at: https://www.ceme.uwa.edu.au/__data/assets/pdf_file/0009/2358270/Fasolo_2013.pdf.

Fukami, T., Wardle, D.A., Bellingham, P.J., *et al.* (2006) ‘Above- and below-ground impacts of introduced predators in seabird-dominated island ecosystems’, *Ecology Letters*, 9(12), pp. 1299–1307. doi:10.1111/J.1461-0248.2006.00983.X.

Garside, C. (1985) ‘The vertical distribution of nitrate in open ocean surface water’, *Deep Sea Research Part A. Oceanographic Research Papers*, 32(6), pp. 723–732. doi:10.1016/0198-0149(85)90075-5.

GEBCO Compilation Group (2021) ‘GEBCO 2021 Grid’, *GEBCO 2021 Grid* [Preprint]. doi:10.5285/c6612cbe-50b3-0cff-e053-6c86abc09f8f.

George, J. v, Nuncio, M., Anilkumar, N., *et al.* (2018) ‘Seasonal Surface Chlorophyll a Variability in the Seychelles–Chagos Thermocline Ridge’, *Current Science*, 114(04), p. 868. doi:10.18520/cs/v114/i04/868-878.

George, J. v, Nuncio, M., Chacko, R., *et al.* (2012) ‘Role of physical processes in chlorophyll distribution in the western tropical Indian Ocean’, *Journal of Marine Systems*, 113–114, pp. 1–12. doi:10.1016/j.jmarsys.2012.12.001.

Goes, J.I. (2020) *RAPID - Assessing the Response of the Seychelles-Chagos Thermocline Ridge Ecosystem to an Indian Ocean Dipole Event - Research Projects - Columbia Climate School*, *Columbia Climate School*. Available at: https://people.climate.columbia.edu/projects/view/2078 (Accessed: 27 July 2022).

Google Earth Pro 7.3.3 (2022) ‘Egmont Atoll, 6°39’46" S, 71°21’26" E’. Available at: http://www.google.com/earth/index.html (Accessed: 15 July 2022).

Gordon, H.R. and McCluney, W.R. (1975) ‘Estimation of the Depth of Sunlight Penetration in the Sea for Remote Sensing’, *Applied Optics*, 14(2), p. 413. doi:10.1364/ao.14.000413.

Gove, J.M., McManus, M.A., Neuheimer, A.B., *et al.* (2016) ‘Near-island Biological Hotspots in Barren Ocean Basins’, *Nature Communications*, 7(1). doi:10.1038/ncomms10581.

Gower, J.F.R. (2014) ‘A simpler picture of satellite chlorophyll fluorescence’, *Remote Sensing Letters*, 5(6), pp. 583–589. doi:10.1080/2150704X.2014.940630.

Graham, N.A.J., Wilson, S.K., Carr, P., *et al.* (2018) ‘Seabirds enhance coral reef productivity and functioning in the absence of invasive rats’, *Nature*, 559(7713), pp. 250–253. doi:10.1038/s41586-018-0202-3.

Gupana, R.S., Odermatt, D., Cesana, I., *et al.* (2021) ‘Remote sensing of sun-induced chlorophyll-a fluorescence in inland and coastal waters: Current state and future prospects’, *Remote Sensing of Environment*, 262, p. 112482. doi:10.1016/J.RSE.2021.112482.

Hamner, W.M. and Hauri, I.R. (1981) ‘Effects of island mass: Water flow and plankton pattern around a reef in the Great Barrier Reef lagoon, Australia’, *Limnology and Oceanography*, 26(6), pp. 1084–1102. doi:10.4319/lo.1981.26.6.1084.

Harris, J.L., Hosegood, P., Robinson, E., *et al.* (2021) ‘Fine-scale oceanographic drivers of reef manta ray (Mobula alfredi) visitation patterns at a feeding aggregation site’, *Ecology and Evolution*, 11(9), pp. 4588–4604. doi:10.1002/ECE3.7357.

Hays, G.C., Koldewey, H.J., Andrzejaczek, S., *et al.* (2020) ‘A review of a decade of lessons from one of the world’s largest MPAs: conservation gains and key challenges’, *Marine Biology*, 167(11), p. 159. doi:10.1007/s00227-020-03776-w.

Head, C.E.I., Bayley, D.T.I., Rowlands, G., *et al.* (2019) ‘Coral bleaching impacts from back-to-back 2015–2016 thermal anomalies in the remote central Indian Ocean’, *Coral Reefs*, 38(4), pp. 605–618. doi:10.1007/s00338-019-01821-9.

Hermes, J.C. and Reason, C.J.C. (2008) ‘Annual cycle of the South Indian Ocean (Seychelles-Chagos) thermocline ridge in a regional ocean model’, *Journal of Geophysical Research*, 113(C4), p. C04035. doi:10.1029/2007JC004363.

Hermes, J.C. and Reason, C.J.C. (2009) ‘The sensitivity of the Seychelles–Chagos thermocline ridge to large-scale wind anomalies’, *ICES Journal of Marine Science*, 66(7), pp. 1455–1466. doi:10.1093/icesjms/fsp074.

Hernández-León, S. (1991) ‘Accumulation of mesozooplankton in a wake area as a causative mechanism of the island-mass effect?’, *Marine Biology*, 109(1), pp. 141–147. doi:10.1007/BF01320241.

Hosegood, P.J., Nimmo-Smith, W.A.M., Proud, R., *et al.* (2019) 'Internal lee waves and baroclinic bores over a tropical seamount shark "hot-spot"', *Progress in Oceanography*, 172, pp. 34–50. doi:10.1016/j.pocean.2019.01.010.

Hsu, J.-Y., Feng, M. and Wijffels, S. (2021) 'Observing Upper Ocean Stratification during Strong Diurnal SST Variation Events in the Suppressed Phase of the MJO'. doi:10.1002/ESSOAR.10506155.1.

Hu, C., Lee, Z. and Franz, B. (2012) 'Chlorophyll a algorithms for oligotrophic oceans: A novel approach based on three-band reflectance difference', *Journal of Geophysical Research: Oceans*, 117(1). doi:10.1029/2011JC007395.

James, A.K., Washburn, L., Gotschalk, C., *et al.* (2020) 'An Island Mass Effect Resolved Near Mo'orea, French Polynesia', *Frontiers in Marine Science*, 7. doi:10.3389/fmars.2020.00016.

Kataoka, T., Kimoto, M., Watanabe, M., *et al.* (2019) 'Wind-mixed layer-SST feedbacks in a tropical air-sea coupled system: Application to the Atlantic', *Journal of Climate*, 32(13), pp. 3865–3881. doi:10.1175/JCLI-D-18-0728.1.

Koldewey, H.J., Curnick, D., Harding, S., *et al.* (2010) 'Potential benefits to fisheries and biodiversity of the Chagos Archipelago/British Indian Ocean Territory as a no-take marine reserve', *Marine Pollution Bulletin*, 60(11), pp. 1906–1915. doi:10.1016/j.marpolbul.2010.10.002.

de La Peña-Lastra, S. (2021) 'Seabird droppings: Effects on a global and local level', *Science of The Total Environment*, 754, p. 142148. doi:10.1016/j.scitotenv.2020.142148.

Lewis, M.R., Harrison, W.G., Oakey, N.S., *et al.* (1986) 'Vertical Nitrate Fluxes in the Oligotrophic Ocean', *Science*, 234(4778), pp. 870–873. doi:10.1126/SCIENCE.234.4778.870.

Martinez, E. and Maamaatuaiahutapu, K. (2004) 'Island mass effect in the Marquesas Islands: Time variation', *Geophysical Research Letters*, 31(18). doi:10.1029/2004gl020682.

Messié, M., Petrenko, A., Doglioli, A.M., *et al.* (2020) 'The Delayed Island Mass Effect: How Islands can Remotely Trigger Blooms in the Oligotrophic Ocean', *Geophysical Research Letters*, 47(2). doi:10.1029/2019gl085282.

Moore, C.M., Mills, M.M., Arrigo, K.R., *et al.* (2013) 'Processes and patterns of oceanic nutrient limitation', *Nature Geoscience*, 6(9), pp. 701–710. doi:10.1038/ngeo1765.

Morel, A., Claustre, H. and Gentili, B. (2010) 'The most oligotrophic subtropical zones of the global ocean: similarities and differences in terms of chlorophyll and yellow substance', *Biogeosciences*, 7(10), pp. 3139–3151. doi:10.5194/bg-7-3139-2010.

Nyadjro, E.S., Jensen, T.G., Richman, J.G., *et al.* (2017) 'On the Relationship Between Wind, SST, and the Thermocline in the Seychelles–Chagos Thermocline Ridge', *IEEE Geoscience and Remote Sensing Letters*, 14(12), pp. 2315–2319. doi:10.1109/LGRS.2017.2762961.

O'reilly, J.E., Maritorena, S., Mitchell, B.G., *et al.* (1998) 'Ocean color chlorophyll algorithms for SeaWiFS', *JOURNAL OF GEOPHYSICAL RESEARCH*, 103, pp. 937–961. doi:10.1029/98JC02160.

Painting, S., Archer-Rand, S., Nelson, P., *et al.* (2019) *Blue Belt Water Quality Expedition Survey Report - Diego Garcia March/April 2019*, *British Indian Ocean Territory*. CEFAS. Available at: https://biot.gov.io/wp-content/uploads/BIOT-WQ-Survey-Report.docx.pdf.

Painting, S.J., Nelson, P., Smith, A.J., *et al.* (2021) 'Marine Water Quality at Diego Garcia: A Preliminary Study of Pollution Levels in Coastal and Lagoon Waters', *Frontiers in Marine Science*, 8. doi:10.3389/fmars.2021.671319.

Praveen Kumar, B., Vialard, J., Lengaigne, M., *et al.* (2014) 'Processes of interannual mixed layer temperature variability in the thermocline ridge of the Indian Ocean', *Climate Dynamics*, 43(9–10), pp. 2377–2397. doi:10.1007/s00382-014-2059-y.

Raitsos, D.E., Pradhan, Y., Brewin, R.J.W., *et al.* (2013) 'Remote Sensing the Phytoplankton Seasonal Succession of the Red Sea', *PLoS ONE*. Edited by I. Álvarez, 8(6). doi:10.1371/journal.pone.0064909.

Reid, E.C., DeCarlo, T.M., Cohen, A.L., *et al.* (2019) 'Internal waves influence the thermal and nutrient environment on a shallow coral reef', *Limnology and Oceanography*, 64(5), pp. 1949–1965. doi:10.1002/lno.11162.

Resplandy, L., Vialard, J., Lévy, M., *et al.* (2009) 'Seasonal and intraseasonal biogeochemical variability in the thermocline ridge of the southern tropical Indian Ocean', *Journal of Geophysical Research: Oceans*, 114(C7), p. 7024. doi:10.1029/2008JC005246.

Rigby, S.J., Williams, R.G., Achterberg, E.P., *et al.* (2020) 'Resource Availability and Entrainment Are Driven by Offsets Between Nutriclines and Winter Mixed-Layer Depth', *Global Biogeochemical Cycles*, 34(7). doi:10.1029/2019gb006497.

Ryabenko, E. (2013) 'Stable Isotope Methods for the Study of the Nitrogen Cycle', in E. Zambianchi (ed.) *Topics in Oceanography*. InTech. doi:10.5772/56105.

Saji, N.H., Goswami, B.N., Vinayachandran, P.N., *et al.* (1999) 'A dipole mode in the tropical Indian Ocean', *Nature*, 401(6751), pp. 360–363. doi:10.1038/43854.

Sallée, J.-B., Pellichero, V., Akhoudas, C., *et al.* (2021) 'Summertime increases in upper-ocean stratification and mixed-layer depth', *Nature*, 591(7851), pp. 592–598. doi:10.1038/s41586-021-03303-x.

Samoilys, M., Roche, R., Koldewey, H., *et al.* (2018) 'Patterns in reef fish assemblages: Insights from the Chagos Archipelago', *PLOS ONE*. Edited by H.M. Patterson, 13(1). doi:10.1371/journal.pone.0191448.

Serôdio, J. and Campbell, D.A. (2021) 'Photoinhibition in optically thick samples: Effects of light attenuation on chlorophyll fluorescence-based parameters', *Journal of Theoretical Biology*, 513, p. 110580. doi:10.1016/J.JTBI.2021.110580.

Shatova, O., Wing, S.R., Gault-Ringold, M., *et al.* (2016) 'Seabird guano enhances phytoplankton production in the Southern Ocean', *Journal of Experimental Marine Biology and Ecology*, 483, pp. 74–87. doi:10.1016/j.jembe.2016.07.004.

Sheehan, E. v, Hosegood, P., Game, C.A., *et al.* (2019) 'The Effect of Deep Oceanic Flushing on Water Properties and Ecosystem Functioning Within Atolls in the British Indian Ocean Territory', *Frontiers in Marine Science*, 6. doi:10.3389/fmars.2019.00512.

Shen, C., Yan, Y., Zhao, H., *et al.* (2018) 'Influence of monsoonal winds on chlorophyll-α distribution in the Beibu Gulf', *PLOS ONE*, 13(1), p. e0191051. doi:10.1371/JOURNAL.PONE.0191051.

Sheppard, C.R.C., Ateweberhan, M., Bowen, B.W., *et al.* (2012) 'Reefs and islands of the Chagos Archipelago, Indian Ocean: why it is the world's largest no-take marine protected area', *Aquatic Conservation: Marine and Freshwater Ecosystems*, 22(2), pp. 232–261. doi:10.1002/AQC.1248.

Sloth, N.P., Riemann, B., Nielsen, L.P., *et al.* (1996) 'Resilience of Pelagic and Benthic Microbial Communities to Sediment Resuspension in a Coastal Ecosystem, Knebel Vig, Denmark', *Estuarine, Coastal and Shelf Science*, 42(4), pp. 405–415. doi:10.1006/ECSS.1996.0027.

Vissa, N.K., Satyanarayana, A.N.V. and Prasad Kumar, B. (2013) 'Comparison of mixed layer depth and barrier layer thickness for the Indian Ocean using two different climatologies', *International Journal of Climatology*, 33(13), pp. 2855–2870. doi:10.1002/JOC.3635.

Webber, B.G.M., Matthews, A.J., Heywood, K.J., *et al.* (2014) 'Seaglider observations of equatorial Indian Ocean Rossby waves associated with the Madden-Julian Oscillation', *Journal of Geophysical Research: Oceans*, 119(6), pp. 3714–3731. doi:10.1002/2013jc009657.

Whalen, C.B., de Lavergne, C., Naveira Garabato, A.C., *et al.* (2020) 'Internal wave-driven mixing: governing processes and consequences for climate', *Nature Reviews Earth & Environment*, 1(11), pp. 606–621. doi:10.1038/s43017-020-0097-z.

Xie, S.-P., Annamalai, H., Schott, F.A., *et al.* (2002) 'Structure and Mechanisms of South Indian Ocean Climate Variability', *Journal of Climate*, 15(8), pp. 864–878. doi:10.1175/1520-0442(2002)015<0864:samosi>2.0.co;2.

Xing, X.G., Zhao, D.Z., Liu, Y.G., *et al.* (2007) 'An overview of remote sensing of chlorophyll fluorescence', *Ocean Science Journal 2007 42:1*, 42(1), pp. 49–59. doi:10.1007/BF03020910.

Zhang, C. (2005) 'Madden-Julian Oscillation', *Reviews of Geophysics*, 43(2). doi:10.1029/2004RG000158.

Zhang, S., Xie, L., Hou, Y., *et al.* (2014) 'Tropical storm-induced Turbulent Mixing and chlorophyll-a Enhancement in the Continental Shelf Southeast of Hainan Island', *Journal of Marine Systems*, 129, pp. 405–414. doi:10.1016/j.jmarsys.2013.09.002.

Zhang, X. and Han, W. (2019) 'Effects of climate modes on interannual variability of upwelling in the tropical Indian Ocean', *Journal of Climate*, 33(4). doi:10.1175/jcli-d-19-0386.1.

Zheng, G.M. and Tang, D.L. (2007) 'Offshore and nearshore chlorophyll increases induced by typhoon winds and subsequent terrestrial rainwater runoff', *Marine Ecology Progress Series*, 333, pp. 61–74. doi:10.3354/meps333061.